Composite Structures 158 (2016) 262–280

Contents lists available at ScienceDirect

Composite Structures

journal homepage: www.elsevier.com/locate/compstruct

Spectral dynamic stiffness formulation for inplane modal analysis of composite plate assemblies and prismatic solids with arbitrary classical/nonclassical boundary conditions

X. Liu [a,b,*]

[a] School of Traffic & Transportation Engineering, Central South University, Changsha 410075, China
[b] School of Mathematics, Computer Sciences and Engineering, City, University of London, London EC1V 0HB, UK

ARTICLE INFO

Article history:
Received 7 July 2016
Revised 26 August 2016
Accepted 12 September 2016
Available online 14 September 2016

Keywords:
Spectral dynamic stiffness method (SDSM)
Inplane modal analysis
Symmetric cross-ply laminated plates
Prismatic orthotropic solids
Non-uniform elastic supports and mass attachments
Non-uniform elastic coupling constraints

ABSTRACT

This paper presents an analytical spectral dynamic stiffness (SDS) formulation for exact inplane modal analysis of composite plate assemblies and prismatic solids subjected to any arbitrary boundary conditions, arbitrary non-uniform elastic supports, mass attachments and coupling constraints. First, the elemental SDS matrix is derived symbolically from the exact general solution of the governing differential equation, which is assembled directly to model complex geometries. Then, any arbitrary classical and/or non-classical boundary conditions are applied directly in a strong form, which makes the method versatile for a wide range of engineering problems. As the solution technique, the Wittrick-Williams algorithm is applied by resolving the mode count problem of a fully clamped element. It is demonstrated that the method gives exact solutions with prominent computational efficiency. The proposed method provides an efficient and accurate analytical tool for the parametric and optimization analysis on the inplane vibration of various composite structures.

1. Introduction

Although the majority of existing investigations have been devoted to the transverse modal analysis of composite plates, there is a growing awareness that inplane vibration plays a significant role in many elastodynamic problems. For example, the inplane vibration should be considered in built-up structures [1–5] since it is generally coupled with out-of-plane vibration when different plates joint at a certain angle. The inplane vibration becomes even more important when the structures are excited within higher frequency range in energy flow and noise transmission analysis [6–10]. Also, inplane modal analysis of plates has been widely used in other areas, such as linear ultrasonic motors [11–14] and shear walls [15–20]. On the other hand, the inplane (cross-sectional) vibration of prismatic solids is generally encountered in structural health monitoring [21–26], seismic analysis of civil engineering structures like dams [27] and buildings, plane strain vibration of composite hollow cylinders [28,29], and edge vibration of laminated plates [30–32].

Nevertheless, compared to transverse vibrations, the existing analytical research on inplane vibrations of composite plates and prismatic solids is scarce which furthermore, has some or other restrictions. Gorman [33] applied the superposition method to conduct the inplane modal analysis of fully clamped orthotropic plates. Wittrick and Williams [1], and Boscolo and Banerjee [34] developed the dynamic stiffness method for the exact free inplane vibration of plates with a pair of opposite edges simply supported. Wang and Wereley [35] solved the free inplane vibration of plates with free and clamped edges using the Kantorovich method. Liu and Xing presented the closed-form exact solutions for free inplane vibration of isotropic [36,37] and orthotropic plates [38] with at least one pair of the plate edges simply supported. Dozio [39] used the Ritz method based on trigonometric functions for the free inplane vibration of symmetric laminated anisotropic plates, where the boundary conditions can be any combination of free and clamped. Ghorbel [40] developed the dynamic stiffness method for the inplane harmonic response of a completely free orthotropic rectangular plate. More recently, Papkov [41] discussed the inplane vibration of completely free and fully clamped rectangular orthotropic plates by investigating the asymptotic behaviour of the formulated non-trivial quasi-regular infinite systems. However, all above methods have been restricted to certain classical boundary conditions (BCs).

* Address: School of Traffic & Transportation Engineering, Central South University, Changsha 410075, China.
E-mail address: xiangliu06@gmail.com

http://dx.doi.org/10.1016/j.compstruct.2016.09.019
0263-8223/

The above restrictions have been removed by some other methods to account for general classical BCs and/or uniform elastic supports. Methods considering general classical BCs include different Ritz methods by Bardell et al. [42] and Dozio [43], dynamic stiffness method by Nefovska-Danilovic and Petronijevic [44] and the spectral collocation method by Mohazzab and Dozio [45]. However, there are much fewer investigations considering inplane vibration subjected to uniform elastic supports. The earliest work on inplane vibration under elastic supports is probably performed by Gorman [46], where the uniform normal elastic supports were treated by using the superposition method. Later, Zhang et al. [47] investigated the free inplane vibration of orthotropic rectangular plates with uniform elastic edges by using the Fourier series based analytical method.

Whilst non-uniform elastic supports are generally used to model more realistic supports, it appears that existing work on inplane vibration of plates subjected to non-uniform elastic supports are sporadic in the literature [43,48] (both using weak-form Ritz methods). Dozio [43] applied the Trigonometric Ritz method for the free inplane analysis of isotropic rectangular plates with arbitrary elastic supports. Shi et al. [48] applied the Ritz method based on an improved Fourier series to allow the treatment of some practical boundary conditions such as uniform elastic supports, point supports, partial supports and internal line supports. However, in both weak-form methods, clamped and simple supports need to be modelled by using the penalty method, whose main drawback [49] lies in choosing a suitable magnitude for the penalty parameter. Furthermore, both research seems to have been limited to single rectangular plates. The modelling of plates with more complex geometries should resort to numerical methods, such as the recently developed differential quadrature finite element method (FEM) by Xing and Liu [50], strong formulation FEM by Fantuzzi and Tornabene [51,52] and the differential quadrature hierarchical FEM by Liu et al. [53]. However, until now the associated theories considering non-uniform elastic supports for these powerful strong-form methods still need to be developed.

To the best of the author's knowledge, there is no existing analytical method in the literature on the inplane vibration of composite plate assemblies or prismatic solids, let alone considering arbitrary non-uniform elastic supports, mass attachments and elastic coupling constraints. However, those cases are more frequently encountered in practical engineering problems. In particular, the non-uniform elastic supports can model more realistic supports with non-uniform stiffness such as damaged boundaries. The non-uniform mass attachments can describe any arbitrary masses that are attached to plate assemblies or solid surfaces, e.g., floors loaded onto shear walls, or sensors attached to structures. The non-uniform elastic coupling constraints can be used to model for example, adhesive layers, cracks or buffer springs between two plates or solids, or the coupling between two shear walls.

Therefore, the major purpose of this paper is to develop an exact but general analytical theory called the spectral dynamic stiffness method (SDSM) for the inplane modal analysis of two types of composite structures. These include both the free inplane vibration of symmetric cross-ply laminated plates and the cross-sectional free vibration of prismatic orthotropic solids. Both the plate assemblies and the cross sections of prismatic solids may have simple or complex geometries. Furthermore, they may be subjected to any arbitrary classical BCs as well as non-classical BCs including, arbitrary non-uniform elastic supports, mass attachments and coupling constraints. The SDS formulations for both elements and classical or non-classical BCs are in a strong form and therefore, are very easy to implemented in computation. The SDSM was first proposed by Liu and Banerjee for the transverse free vibration of isotropic plates [54] and composite plate assemblies [55,56] and later for plane elastodynamic problems [57]. Also, an SDS theory has been proposed to deal with the transverse vibration of plate assemblies with any arbitrary elastic supports, mass attachments and coupling constraints [58]. However, the SDS formulation has not been developed for the inplane vibration of composite plate assemblies and prismatic solids with arbitrary classical and/or nonclassical BCs. Besides, it will also be shown that the SDSM gives exact results with excellent computational efficiency, which exhibits a predominant advantage over the FEM and other methods in terms of accuracy and computational efficiency. All results computed by the SDSM are accurate up to the last digit presented, which will serve as benchmark solutions.

The paper is organised as follows. In Section 2.1, the governing different equation (GDE) and the natural boundary conditions (BCs) of inplane vibration problems are formulated using Hamilton's principle. This is followed by the development of exact general solution of the GDE (Section 2.2) and the spectral representation of any arbitrary BCs (Section 2.3). Then, the spectral dynamic stiffness formulation for an element is developed which then can be assembled directly to model complex structures, see Section 3. The corresponding SDS theory dealing with any arbitrary non-uniform elastic supports, mass attachments and coupling constraints is given in Section 4. In Section 5, as a solution technique, the Wittrick-William algorithm is enhanced by resolving the mode count problem of a fully clamped element. In order to assist readers who are interested in applying the proposed method, Section 6 describes the implementation procedure in details. Then in Section 7, the proposed method is validated against existing results wherever available and then applied to a wide range of engineering problems. Finally, the paper is concluded in Section 8.

2. Preliminaries

2.1. Derivation of governing differential equation and boundary conditions

First, the governing differential equation and the corresponding natural boundary conditions are derived using Hamilton's principle. Assume that the geometry, material and the prescribed boundary conditions of a three-dimensional elastic body are uniform in one direction, such that all deformation and forces can be represented by the displacement of its cross section occupying the region Ω bounded by $\partial\Omega$. If the deformation field of this cross section is described by $\boldsymbol{u}$, Hamilton's principle in the usual notation gives

$$\delta \int_{t_1}^{t_2} (\mathcal{K} - \mathcal{W} + \mathcal{W}_e)\mathrm{d}t = 0, \tag{1}$$

where $\mathcal{K}$ and $\mathcal{W}$ are the kinetic energy and elastic energies respectively, and $\mathcal{W}_e$ is the work done by external loads $\boldsymbol{t}$ on the $\partial\Omega$ (assuming no body force is applied). If the elastic body is under small deformation, e.g., $|\boldsymbol{u}| \ll 1$ then

$$\mathcal{K} = \frac{1}{2}\int_\Omega \rho \dot{\boldsymbol{u}} \cdot \dot{\boldsymbol{u}} \mathrm{d}A, \quad \mathcal{W} = \frac{1}{2}\int_\Omega \boldsymbol{\sigma} : \boldsymbol{e} \mathrm{d}A, \quad \mathcal{W}_e = \int_{\partial\Omega} \boldsymbol{t} \cdot \boldsymbol{u} \mathrm{d}s,$$

where $\boldsymbol{\sigma}$ is the Cauchy stress tensor

$$\boldsymbol{\sigma} = \mathbb{C} : \boldsymbol{e}, \quad \boldsymbol{e} = \frac{1}{2}(\boldsymbol{u} \otimes \boldsymbol{\nabla} + \boldsymbol{\nabla} \otimes \boldsymbol{u}) = (\boldsymbol{\nabla} \otimes \boldsymbol{u})^s, \tag{2}$$

and in which $\mathbb{C}$ is a fourth-order tensor defining the *reduced stiffnesses* of the cross section. The corresponding matrix forms of the reduced stiffnesses for an orthotropic material are detailed in Appendix A, which take different expressions for plane stress and plane strain deformations. By using integration by parts, we have

$$\delta\int_{t_1}^{t_2}\mathcal{K}\mathrm{d}t=\int_{\Omega}\rho\dot{\boldsymbol{u}}\cdot\boldsymbol{u}\mathrm{d}A\Big|_{t_1}^{t_2}-\int_{t_1}^{t_2}\left[\int_{\Omega}\rho\ddot{\boldsymbol{u}}\cdot\delta\boldsymbol{u}\mathrm{d}A\right]\mathrm{d}t \tag{3}$$

where the first term on the right hand side evaluated at initial and final time is set to zero according to the Hamilton's principle. Also,

$$\delta\mathcal{W}=\delta\left(\frac{1}{2}\int_{\Omega}\boldsymbol{e}:\mathbb{C}:\boldsymbol{e}\mathrm{d}A\right)=\int_{\Omega}\boldsymbol{\sigma}:\boldsymbol{e}\mathrm{d}A=\int_{\Omega}\boldsymbol{\sigma}:(\boldsymbol{\nabla}\otimes\delta\boldsymbol{u})^{s}\mathrm{d}A. \tag{4}$$

In view of the identity $\boldsymbol{T}:(\boldsymbol{\nabla}\otimes\boldsymbol{a})=\boldsymbol{\nabla}\cdot(\boldsymbol{T}\cdot\boldsymbol{a})-(\boldsymbol{\nabla}\cdot\boldsymbol{T})\cdot\boldsymbol{a}$ which is valid for any second-order tensor $\boldsymbol{T}$ and first-order tensor $\boldsymbol{a}$ and noticing that $\boldsymbol{\sigma}$ is a symmetric tensor, the expression on the right hand side of Eq. (4) can be rewritten as

$$\int_{\Omega}[\boldsymbol{\nabla}\cdot(\boldsymbol{\sigma}\cdot\delta\boldsymbol{u})-(\boldsymbol{\nabla}\cdot\boldsymbol{\sigma})\cdot\delta\boldsymbol{u}]\mathrm{d}A=\int_{\partial\Omega}(\boldsymbol{\sigma}\cdot\boldsymbol{n})\cdot\delta\boldsymbol{u}\mathrm{d}s-\int_{\Omega}(\boldsymbol{\nabla}\cdot\boldsymbol{\sigma})\cdot\delta\boldsymbol{u}\mathrm{d}A. \tag{5}$$

Assuming that the boundary forces $\boldsymbol{t}$ are dead loads, one has

$$\delta\int_{t_1}^{t_2}\mathcal{W}_e\mathrm{d}t=\int_{t_1}^{t_2}\left[\int_{\partial\Omega}\boldsymbol{t}\cdot\delta\boldsymbol{u}\mathrm{d}s\right]\mathrm{d}t. \tag{6}$$

Substituting Eqs. (3), (5) and (6) into Eq. (1) leads to

$$\delta\int_{t_1}^{t_2}\left[\int_{\Omega}(\boldsymbol{\nabla}\cdot\boldsymbol{\sigma}-\rho\ddot{\boldsymbol{u}})\cdot\delta\boldsymbol{u}\mathrm{d}A+\int_{\partial\Omega}(\boldsymbol{t}-\boldsymbol{\sigma}\cdot\boldsymbol{n})\cdot\delta\boldsymbol{u}\mathrm{d}A\right]\mathrm{d}t=0. \tag{7}$$

In view of Eq. (2), we have

$$\boldsymbol{\nabla}\cdot\boldsymbol{\sigma}=\boldsymbol{\nabla}\cdot(\mathbb{C}:\boldsymbol{e})=\mathbb{C}\dot{:}(\boldsymbol{\nabla}\otimes\boldsymbol{e})=\mathbb{C}\dot{:}\boldsymbol{\nabla}\otimes(\boldsymbol{\nabla}\otimes\boldsymbol{u})^{s}. \tag{8}$$

Now we introduce the local coordinates $\{\boldsymbol{n},\boldsymbol{s}\}$ attached to the boundary $\partial\Omega$, where $\boldsymbol{n}$ and $\boldsymbol{s}$ are normal and tangent unit vectors which form a local orthonormal basis. Therefore, the second term in the square brackets on the left hand side of Eq. (7) becomes

$$\int_{\partial\Omega}(\boldsymbol{t}-\boldsymbol{\sigma}\cdot\boldsymbol{n})\cdot\delta\boldsymbol{u}\mathrm{d}s=\int_{\partial\Omega}(\boldsymbol{t}-\boldsymbol{\sigma}\cdot\boldsymbol{n})\cdot(\delta u_n\boldsymbol{n}+\delta u_s\boldsymbol{s})\mathrm{d}s. \tag{9}$$

Due to the arbitrariness of $\delta\boldsymbol{u}$ in Eq. (7), the governing equation of the above system can be cast as

$$\mathbb{C}\dot{:}\boldsymbol{\nabla}\otimes(\boldsymbol{\nabla}\otimes\boldsymbol{u})^{s}-\rho\ddot{\boldsymbol{u}}=0. \tag{10}$$

and the natural boundary condition can be written in the form

$$\delta u_n:\quad t_n=\mathbb{C}:(\boldsymbol{\nabla}\otimes\boldsymbol{u})^{s}\cdot\boldsymbol{n}\cdot\boldsymbol{n}, \tag{11a}$$

$$\delta u_s:\quad t_s=\mathbb{C}:(\boldsymbol{\nabla}\otimes\boldsymbol{u})^{s}\cdot\boldsymbol{n}\cdot\boldsymbol{s}, \tag{11b}$$

where $t_n=\boldsymbol{t}\cdot\boldsymbol{n}$ and $t_s=\boldsymbol{t}\cdot\boldsymbol{s}$. The component form of Eq. (10) can be written as

$$\frac{1}{2}\mathbb{C}^{\alpha\beta\gamma\delta}(\Delta_\beta\Delta_\delta u_\gamma+\Delta_\beta\Delta_\gamma u_\delta)-\rho\ddot{u}^{\alpha}=0 \tag{12}$$

By considering Eqs. (2) and (7), the component form of the natural BCs in Eq. (11) takes the form

$$\delta u_n:\quad t_n=\frac{1}{2}\mathbb{C}^{\alpha\beta\gamma\delta}(\Delta_\delta u_\gamma+\Delta_\gamma u_\delta)n_\beta n_\alpha, \tag{13a}$$

$$\delta u_s:\quad t_s=\frac{1}{2}\mathbb{C}^{\alpha\beta\gamma\delta}(\Delta_\delta u_\gamma+\Delta_\gamma u_\delta)n_\beta s_\alpha. \tag{13b}$$

2.2. Governing differential equation and exact general solution

If the displacement field $\boldsymbol{u}$ within the domain Ω is assumed to undergo harmonic oscillation such that $\boldsymbol{u}=[U(x,y),V(x,y)]^T\exp(i\omega t)$, then the governing differential equation (GDE) for the inplane vibration of an element in the frequency domain is given by

$$a_1U_{,xx}+U_{,yy}+(a_3+1)V_{,xy}+\kappa U=0, \tag{14a}$$

$$a_2V_{,yy}+V_{,xx}+(a_3+1)U_{,xy}+\kappa V=0, \tag{14b}$$

where the suffix after the comma denotes the related partial derivatives and

$$a_1=\frac{A_{11}}{A_{66}},\ a_2=\frac{A_{22}}{A_{66}},\ a_3=\frac{A_{12}}{A_{66}},\ \kappa=\frac{I_0\omega^2}{A_{66}}. \tag{15}$$

Note that Eq. (14) applies for the inplane vibration of both symmetric cross-ply plates (under plane stress assumption) and infinite prismatic orthotropic solids (under plane strain assumption). For the plane stress case, when a symmetric cross-ply plate is composed of N_l layers, the material parameters of Eq. (15) are given as follows

$$A_{ij}=\sum_{k=1}^{N_l}\overline{Q}_{ij}^{(k)}h^{(k)},\quad I_0=\sum_{k=1}^{N_l}\rho^{(k)}h^{(k)}, \tag{16}$$

where the superscript $k\in\{1,2,\ldots,N_l\}$ denotes the kth layer of the total N_l layers. For the plane strain vibration of an infinite prismatic orthotropic solid, the parameters of Eq. (15) become

$$A_{ij}=\overline{Q}_{ij},\quad I_0=\rho. \tag{17}$$

Notice that $\overline{Q}_{ij}$ in Eq. (16) or (17) stands for *reduced stiffnesses* in the global coordinates for either plane-stress (Eq. (16)) or plane-strain (Eq. (17)) vibration, which can be transformed from the reduced stiffnesses Q_{ij} in the material reference system following the usual steps as described in [59]. The reduced stiffnesses in the material reference system Q_{ij} take different expressions in plane stress and plane strain, which are provided in Appendix A.

Now we are in position to derive the exact general solution of the GDE (14). With the help of the two sets of modified Fourier basis functions given in Appendix B, the general solution of the GDE (14) can be appropriately represented as follows

$$U(x,y)=\sum_{\substack{m\in\mathbb{N}\\k\in\{0,1\}}}\mathcal{T}_k^*(\alpha_{km}x)U_{km}(y)+\sum_{\substack{n\in\mathbb{N}\\j\in\{0,1\}}}U_{jn}(x)\mathcal{T}_j(\beta_{jn}y), \tag{18a}$$

$$V(x,y)=\sum_{\substack{m\in\mathbb{N}\\k\in\{0,1\}}}\mathcal{T}_k(\alpha_{km}x)V_{km}(y)+\sum_{\substack{n\in\mathbb{N}\\j\in\{0,1\}}}V_{jn}(x)\mathcal{T}_j^*(\beta_{jn}y), \tag{18b}$$

where $\mathcal{T}_k,\mathcal{T}_j$ and $\mathcal{T}_k^*,\mathcal{T}_j^*$ are the modified Fourier basis functions defined by Eqs. (B.1a) and (B.1b) respectively. The corresponding wavenumbers are taken as $\alpha_{km}=(m+k/2)\pi/a$ and $\beta_{jn}=(n+j/2)\pi/b$ with $n\in\mathbb{N}$ and $\mathbb{N}=\{0,1,2,\ldots\}$. It is worth highlighting that the $\mathcal{T}_k,\mathcal{T}_j$ and $\mathcal{T}_k^*,\mathcal{T}_j^*$ are adopted in the way of Eq. (18) such that the k (related to x direction) and j (related to y direction) correspond to the correct symmetry/antisymmetry of the deformation in the related directions. In Eq. (18), $U_{km}(y),U_{jn}(x),V_{km}(y)$ and $V_{jn}(x)$ are unknown functions which are determined by substituting Eq. (18) into the GDE of Eq. (14) to give

$$\begin{bmatrix}\mathrm{d}_y^2+\kappa-a_1\alpha_{km}^2 & -\mu_1\mathrm{d}_y\\ \mu_1\mathrm{d}_y & a_2\mathrm{d}_y^2+\kappa-\alpha_{km}^2\end{bmatrix}\begin{bmatrix}U_{km}(y)\\V_{km}(y)\end{bmatrix}=\begin{bmatrix}0\\0\end{bmatrix}$$
$$(\forall)k\in\{0,1\},\ m\in\mathbb{N}\ \text{except}\ k=m=0 \tag{19a}$$

$$\begin{bmatrix}a_1\mathrm{d}_x^2+\kappa-\beta_{jn}^2 & \mu_2\mathrm{d}_x\\ -\mu_2\mathrm{d}_x & \mathrm{d}_x^2+\kappa-a_2\beta_{jn}^2\end{bmatrix}\begin{bmatrix}U_{jn}(x)\\V_{jn}(x)\end{bmatrix}=\begin{bmatrix}0\\0\end{bmatrix}$$
$$(\forall)j\in\{0,1\},\ n\in\mathbb{N}\ \text{except}\ j=n=0 \tag{19b}$$

where $\mathrm{d}_x^i = \mathrm{d}^i/\mathrm{d}x^i$, $\mathrm{d}_y^i = \mathrm{d}^i/\mathrm{d}y^i$ and $\mu_1 = (-1)^k(a_3+1)\alpha_{km}$, $\mu_2 = (-1)^j(a_3+1)\beta_{jn}$. (Two special cases when $k=m=0$ and $j=n=0$ will be discussed later.) By assuming $U_{km}(y) = \delta_{km}V_{km}(y)$, $V_{km}(y) = \exp(t_{km}y)$ and $V_{jn}(x) = \delta_{jn}U_{jn}(x)$, $U_{jn}(x) = \exp(r_{jn}x)$, the general solutions for $U_{km}(y)$, $V_{km}(y)$, $U_{jn}(x)$ and $V_{jn}(x)$ in Eq. (18) are determined to be

$$\begin{cases} U_{km}(y) = \delta_{1km}\widetilde{C}_{1km}\mathrm{ch}(t_{1km}y) + \delta_{1km}\widetilde{C}_{2km}\mathrm{sh}(t_{1km}y) \\ \qquad +\delta_{2km}\widetilde{C}_{3km}\mathrm{ch}(t_{2km}y) + \delta_{2km}\widetilde{C}_{4km}\mathrm{sh}(t_{2km}y) \\ V_{km}(y) = \widetilde{C}_{1km}\mathrm{ch}(t_{1km}y) + \widetilde{C}_{2km}\mathrm{sh}(t_{1km}y) + \widetilde{C}_{3km}\mathrm{ch}(t_{2km}y) \\ \qquad +\widetilde{C}_{4km}\mathrm{sh}(t_{2km}y) \end{cases} \tag{20a}$$

$$\begin{cases} U_{jn}(x) = \widetilde{D}_{1jn}\mathrm{ch}(r_{1jn}x) + \widetilde{D}_{2jn}\mathrm{sh}(r_{1jn}x) + \widetilde{D}_{3jn}\mathrm{ch}(r_{2jn}x) + \widetilde{D}_{4jn}\mathrm{sh}(r_{2jn}x) \\ V_{jn}(x) = \delta_{1jn}\widetilde{D}_{1jn}\mathrm{ch}(r_{1jn}x) + \delta_{1jn}\widetilde{D}_{2jn}\mathrm{sh}(r_{1jn}x) + \delta_{2jn}\widetilde{D}_{3jn}\mathrm{ch}(r_{2jn}x) \\ \qquad +\delta_{2jn}\widetilde{D}_{4jn}\mathrm{sh}(r_{2jn}x) \end{cases} \tag{20b}$$

where

$$\left.\begin{matrix} t_{1km} \\ t_{2km} \end{matrix}\right\} = \sqrt{\frac{-b_2 \mp \sqrt{b_2^2 - 4a_2c_2}}{2a_2}}, \quad \left.\begin{matrix} r_{1jn} \\ r_{2jn} \end{matrix}\right\} = \sqrt{\frac{-b_1 \mp \sqrt{b_1^2 - 4a_1c_1}}{2a_1}} \tag{21}$$

with

$$b_2 = (a_1+1)\kappa + [a_3(a_3+2) - a_1a_2]\alpha_{km}^2, \quad c_2 = (\kappa - a_1\alpha_{km}^2)(\kappa - \alpha_{km}^2),$$

$$b_1 = (a_1+1)\kappa + [a_3(a_3+2) - a_1a_2]\beta_{jn}^2, \quad c_1 = (\kappa - \beta_{jn}^2)(\kappa - a_2\beta_{jn}^2).$$

Also, by inserting Eq. (20) into Eq. (19), the expressions for δ_{ikm} and δ_{ijn} $(i=1,2)$ in Eq. (20) are obtained to be

$$\delta_{ikm} = -\frac{a_2t_{ikm}^2 + \kappa - \alpha_{km}^2}{\mu_1 t_{ikm}}, \quad \delta_{ijn} = -\frac{a_1r_{ijn}^2 + \kappa - \beta_{jn}^2}{\mu_2 r_{ijn}} \tag{22}$$

together with the following identities

$$\begin{aligned} &(a_1r_{ijn}^2 + \kappa - \beta_{jn}^2)(r_{ijn}^2 + \kappa - a_2\beta_{jn}^2) + \mu_2^2 r_{ijn}^2 = 0, \\ &(t_{ikm}^2 + \kappa - a_1\alpha_{km}^2)(a_2t_{ikm}^2 + \kappa - \alpha_{km}^2) + \mu_1^2 t_{ikm}^2 = 0. \end{aligned} \tag{23}$$

By considering the symmetry/antisymmetry of the hyperbolic and trigonometric functions, the general solution of Eq. (20) can be decomposed into four components

$$U(x,y) = \sum_{k,j\in\{0,1\}} U^{kj}(x,y) = U^{00} + U^{01} + U^{10} + U^{11}, \tag{24a}$$

$$V(x,y) = \sum_{k,j\in\{0,1\}} V^{kj}(x,y) = V^{00} + V^{01} + V^{10} + V^{11}, \tag{24b}$$

k,j taking in turn 0 and 1 denotes symmetric and antisymmetric functions respectively. Therefore,

$$\begin{aligned} U^{kj}(x,y) = &\sum_{m\in\mathbb{N}}\left[\mathcal{T}_k^*(\alpha_{km}x)\sum_{i=1,2}\left(\delta_{1i}C_{ikm}\mathcal{H}_j(t_{ikm}y)\right)\right] \\ &+\sum_{n\in\mathbb{N}}\left[\sum_{i=1,2}\left(D_{ijn}\mathcal{H}_k^*(r_{ijn}x)\right)\mathcal{T}_j(\beta_{jn}y)\right], \end{aligned} \tag{25a}$$

$$\begin{aligned} V^{kj}(x,y) = &\sum_{m\in\mathbb{N}}\left[\mathcal{T}_k(\alpha_{km}x)\sum_{i=1,2}\left(C_{ikm}\mathcal{H}_j^*(t_{ikm}y)\right)\right] \\ &+\sum_{n\in\mathbb{N}}\left[\sum_{i=1,2}\left(\delta_{2i}D_{ijn}\mathcal{H}_k(r_{ijn}x)\right)\mathcal{T}_j^*(\beta_{jn}y)\right], \end{aligned} \tag{25b}$$

where $\mathcal{H}_k, \mathcal{H}_j$ and $\mathcal{H}_k^*, \mathcal{H}_j^*$ stand for hyperbolic functions defined as follows

$$\mathcal{H}_l(\Gamma\xi) = \begin{cases} \mathrm{ch}(\Gamma\xi) & l=0 \\ \mathrm{sh}(\Gamma\xi) & l=1 \end{cases}, \quad \mathcal{H}_l^*(\Gamma\xi) = \begin{cases} \mathrm{sh}(\Gamma\xi) & l=0 \\ \mathrm{ch}(\Gamma\xi) & l=1 \end{cases} \tag{26}$$

with either $l=k$, $\Gamma = r_{ijn}$, $\xi = x$ or $l=j$, $\Gamma = t_{ikm}$, $\xi = y$. However, for the two special cases when $k=m=0$ and $j=n=0$ in Eq. (19), the above development from Eqs. (19) to (25) will be reduced. In particular, both Eqs. (19a) and (19b) will be reduced to second-order equations leading to two roots $\mp t_{00}$ and $\mp r_{00}$ respectively, where

$$t_{00} = \sqrt{-\kappa/a_2}, \quad r_{00} = \sqrt{-\kappa/a_1}. \tag{27}$$

To this end, when $j=n=0$, the first term of the second series on the right hand side of Eq. (25a) becomes $D_{00}\mathcal{H}^*(r_{00}x)$; and when $k=m=0$, the first term of the first series on the right hand side of Eq. (25b) becomes $C_{00}\mathcal{H}^*(t_{00}y)$. In Eq. (25), C_{ikm} and D_{ijn} (including C_{00} and D_{00}) are unknowns to be determined later in Section 3.1.

2.3. Natural boundary conditions and its spectral representation

The natural BCs in the frequency domain along the four boundaries $\mathcal{B}_i$ (i = 1,2,3,4) of the rectangular element in Fig. 1 are obtained by applying Eq. (13) to the four boundaries to give

$$\delta L_i: \ N_i, \quad \delta T_i: \ S_i, \quad i = 1,2,3,4, \tag{28}$$

where the direction of L_i, N_i, T_i and S_i are defined in Fig. 1 with the following expressions

$$\begin{bmatrix} L_1 \\ T_1 \\ L_2 \\ T_2 \\ L_3 \\ T_3 \\ L_4 \\ T_4 \end{bmatrix} = \begin{bmatrix} U|_{x=a} \\ V|_{x=a} \\ V|_{y=b} \\ U|_{y=b} \\ U|_{x=-a} \\ V|_{x=-a} \\ V|_{y=-b} \\ U|_{y=-b} \end{bmatrix}, \quad \begin{bmatrix} N_1 \\ S_1 \\ N_2 \\ S_2 \\ N_3 \\ S_3 \\ N_4 \\ S_4 \end{bmatrix} = A_{66}\begin{bmatrix} (a_1U_{,x} + a_3V_{,y})|_{x=a} \\ (U_{,y} + V_{,x})|_{x=a} \\ (a_2V_{,y} + a_3U_{,x})|_{y=b} \\ (U_{,y} + V_{,x})|_{y=b} \\ -(a_1U_{,x} + a_3V_{,y})|_{x=-a} \\ -(U_{,y} + V_{,x})|_{x=-a} \\ -(a_2V_{,y} + a_3U_{,x})|_{y=-b} \\ -(U_{,y} + V_{,x})|_{y=-b} \end{bmatrix}. \tag{29}$$

Here, L_i and T_i are introduced to denote the normal u_n and tangent u_s displacements respectively of Eq. (13) along the ith boundary $\mathcal{B}_i$; whereas N_i and S_i are the longitudinal t_n and shear t_s forces along $\mathcal{B}_i$. (Note that $L_i(N_i)$ and $T_i(S_i)$ are defined either by $U(\sigma_{xx})$ and $V(\sigma_{xy})$ or by $V(\sigma_{yy})$ and $U(\sigma_{xy})$, depending on which boundary they apply to.) Therefore, there is a 90°phase difference between L_i (N_i) and T_i (S_i), so two types of modified Fourier series (MFS) of Eqs.

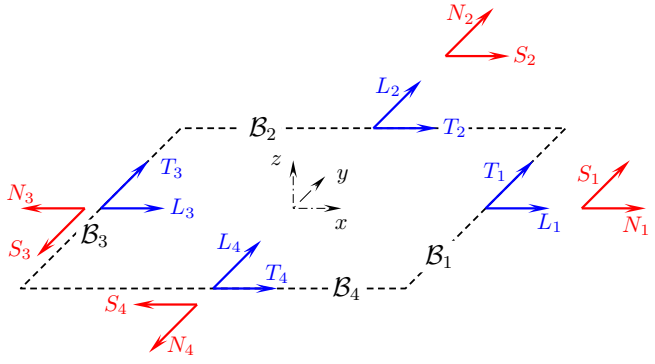

Fig. 1. Coordinate system boundary force and displacement notations for the inplane vibration of an element.

(B.1a) and (B.1b) are adopted to transform any arbitrarily prescribed BCs L_i, N_i and T_i, S_i respectively. To this end, one has the corresponding modified Fourier coefficient vectors

$$\boldsymbol{f} = \left[\boldsymbol{N}_1^T, \boldsymbol{S}_1^T, \boldsymbol{N}_2^T, \boldsymbol{S}_2^T, \boldsymbol{N}_3^T, \boldsymbol{S}_3^T, \boldsymbol{N}_4^T, \boldsymbol{S}_4^T\right]^T, \tag{30a}$$

$$\boldsymbol{d} = \left[\boldsymbol{L}_1^T, \boldsymbol{T}_1^T, \boldsymbol{L}_2^T, \boldsymbol{T}_2^T, \boldsymbol{L}_3^T, \boldsymbol{T}_3^T, \boldsymbol{L}_4^T, \boldsymbol{T}_4^T\right]^T, \tag{30b}$$

where

$$\boldsymbol{N}_i = [N_{i00}, N_{i01}, \ldots, N_{i0s}, \ldots, N_{i10}, N_{i11}, \ldots, N_{i1s}, \ldots]^T, \tag{31a}$$

$$\boldsymbol{S}_i = [S_{i01}, \ldots, S_{i0s}, \ldots, S_{i10}, S_{i11}, \ldots, S_{i1s}, \ldots]^T, \tag{31b}$$

$$\boldsymbol{L}_i = [L_{i00}, L_{i01}, \ldots, L_{i0s}, \ldots, L_{i10}, L_{i11}, \ldots, L_{i1s}, \ldots]^T, \tag{31c}$$

$$\boldsymbol{T}_i = [T_{i01}, \ldots, T_{i0s}, \ldots, T_{i10}, T_{i11}, \ldots, T_{i1s}, \ldots]^T. \tag{31d}$$

Here, the sub-vectors $\boldsymbol{N}_i$ and $\boldsymbol{L}_i$ are the modified Fourier coefficient vectors of the BCs on $\mathcal{B}_i$ of the element by applying the first type of MFS (B.1a) to N_i and L_i of Eq. (29) respectively, and $\boldsymbol{S}_i$ and $\boldsymbol{T}_i$ are the corresponding modified Fourier coefficient vectors by applying the second type of MFS (B.1b) to S_i and T_i of Eq. (29) respectively. For example,

$$N_{ils} = \int_{-L}^{L} \frac{N_i}{A_{66}} \frac{\mathcal{T}_l(\gamma_{ls}\xi)}{\sqrt{\zeta_{ls}L}} \mathrm{d}\xi, \quad T_{ils} = \int_{-L}^{L} T_i \frac{\mathcal{T}_l^*(\gamma_{ls}\xi)}{\sqrt{\zeta_{ls}L}} \mathrm{d}\xi,$$

where $l \in \{0,1\}, s \in \mathbb{N}, \xi$ denotes either x or y and $2L$ is the boundary length representing either $2a$ or $2b$ in this paper. It should be noted that S_{i00} and T_{i00} are zero because $\mathcal{T}_0^*(\gamma_{00}\xi) \equiv 0$ based on Eq. (B.1b). Therefore, both S_{i00} and T_{i00} have been deleted from the vectors $\boldsymbol{S}_i$ and $\boldsymbol{T}_i$ respectively to avoid null rows or columns.

3. Development of the spectral dynamic stiffness matrix for inplane vibration

Since the general solution of Eq. (18) can be decomposed into four (k,j) components as in Eq. (25), the spectral dynamic stiffness (SDS) matrix $\boldsymbol{K}$ of a rectangular element also can be combined by the corresponding four (k,j) SDS components $\boldsymbol{K}^{kj}$ where $k,j \in \{0,1\}$. The development of the SDS component matrix $\boldsymbol{K}^{kj}$ are performed in Section 3.1 which are then combined to form the complete SDS matrix $\boldsymbol{K}$ of an entire element, see Section 3.2. Finally, Section 3.3 describes briefly the assembly procedure for the final structure and the application of arbitrary classical boundary condition.

3.1. Development of the SDS component matrix $\boldsymbol{K}^{kj}$

Similar to the SDSM development for transverse vibration of thin plates [55], the SDS component matrix $\boldsymbol{K}^{kj}$ for inplane vibration is also developed by eliminating the unknowns in the corresponding (k,j) component of the general solution given in Eq. (25). This is achieved by expressing the (k,j) component of the natural BCs given in Eq. (29) as follows

$$\begin{bmatrix} L_a^{kj} \\ L_b^{kj} \\ T_a^{kj} \\ T_b^{kj} \end{bmatrix} = \begin{bmatrix} U^{kj}|_{x=a} \\ V^{kj}|_{y=b} \\ V^{kj}|_{x=a} \\ U^{kj}|_{y=b} \end{bmatrix} = \begin{bmatrix} \sum_{n\in\mathbb{N}} L_{ajn} \frac{\mathcal{T}_j(\beta_{jn}y)}{\sqrt{\zeta_{jn}b}} \\ \sum_{m\in\mathbb{N}} L_{bkm} \frac{\mathcal{T}_k(\alpha_{km}x)}{\sqrt{\zeta_{km}a}} \\ \sum_{n\in\mathbb{N}} T_{ajn} \frac{\mathcal{T}_j^*(\beta_{jn}y)}{\sqrt{\zeta_{jn}b}} \\ \sum_{m\in\mathbb{N}} T_{bkm} \frac{\mathcal{T}_k^*(\alpha_{km}x)}{\sqrt{\zeta_{km}a}} \end{bmatrix}, \tag{32a}$$

$$\begin{bmatrix} N_a^{kj} \\ N_b^{kj} \\ S_a^{kj} \\ S_b^{kj} \end{bmatrix} = A_{66} \begin{bmatrix} a_1 U_{,x}^{kj} + a_3 V_{,y}^{kj}|_{x=a} \\ a_2 V_{,y}^{kj} + a_3 U_{,x}^{kj}|_{y=b} \\ U_{,y}^{kj} + V_{,x}^{kj}|_{x=a} \\ U_{,y}^{kj} + V_{,x}^{kj}|_{y=b} \end{bmatrix} = A_{66} \begin{bmatrix} \sum_{n\in\mathbb{N}} N_{ajn} \frac{\mathcal{T}_j(\beta_{jn}y)}{\sqrt{\zeta_{jn}b}} \\ \sum_{m\in\mathbb{N}} N_{bkm} \frac{\mathcal{T}_k(\alpha_{km}x)}{\sqrt{\zeta_{km}a}} \\ \sum_{n\in\mathbb{N}} S_{ajn} \frac{\mathcal{T}_j^*(\beta_{jn}y)}{\sqrt{\zeta_{jn}b}} \\ \sum_{m\in\mathbb{N}} S_{bkm} \frac{\mathcal{T}_k^*(\alpha_{km}x)}{\sqrt{\zeta_{km}a}} \end{bmatrix} \tag{32b}$$

In consequence, the unknowns D_{1jn} and D_{2jn} in the (k,j) general solution component of Eq. (25) can be determined from the expressions L_a^{kj} of Eq. (32a) and S_a^{kj} of Eq. (32b). In this way,

$$U^{kj}\Big|_{x=a} = \sum_{n\in\mathbb{N}} L_{ajn} \mathcal{T}_j(\beta_{jn}y)/\sqrt{\zeta_{jn}b}, \tag{33a}$$

$$U_{,y}^{kj} + V_{,x}^{kj}\Big|_{x=a} = \sum_{n\in\mathbb{N}} S_{ajn} \mathcal{T}_j^*(\beta_{jn}y)/\sqrt{\zeta_{jn}b}, \tag{33b}$$

which yield

$$\sum_{i=1,2} \left[D_{ijn} \mathcal{H}_k^*(r_{ijn}a)\right] = L_{ajn}/\sqrt{\zeta_{jn}b}, \tag{34a}$$

$$\sum_{i=1,2} \left[\left((-1)^{j+1}\beta_{jn} + \delta_{2i} r_{ijn}\right) D_{ijn} \mathcal{H}_k^*(r_{ijn}a)\right] = S_{ajn}/\sqrt{\zeta_{jn}b} \tag{34b}$$

$(\forall) k,j \in \{0,1\}, n \in \mathbb{N}$ except for $n = j = 0$ when Eq. (34a) becomes $D_{00}\mathcal{H}_k^*(r_{00}a) = L_{a00}/\sqrt{2b}$. Then the unknown coefficients D_{00}, D_{1jn} and D_{2jn} can be determined from Eq. (34) to give

$$D_{00} = \frac{L_{a00}}{\sqrt{2b}\mathcal{H}_k^*(r_{00}a)} \quad j = n = 0 \tag{35a}$$

$$\left.\begin{aligned} D_{1jn} &= \frac{\left[(-1)^{j+1}\beta_{jn} + \delta_{22} r_{2jn}\right] L_{ajn} - S_{ajn}}{\sqrt{\zeta_{jn}b}\mathcal{H}_k^*(r_{1jn}a)\Xi_2/\mu_2} \\ D_{2jn} &= -\frac{\left[(-1)^{j+1}\beta_{jn} + \delta_{21} r_{1jn}\right] L_{ajn} - S_{ajn}}{\sqrt{\zeta_{jn}b}\mathcal{H}_k^*(r_{2jn}a)\Xi_2/\mu_2} \end{aligned}\right\} \quad \text{otherwise}, \tag{35b}$$

where $\Xi_2 = (a_2\beta_{jn}^2 - \kappa)(r_{1jn}^2 - r_{2jn}^2)/(r_{1jn}r_{2jn})$. Similarly, the expressions of L_b^{kj} in Eq. (32a) and S_b^{kj} in Eq. (32b) yield the unknowns C_{00}, C_{1km} and C_{2km} to be

$$C_{00} = \frac{L_{b00}}{\sqrt{2a}\mathcal{H}_j^*(t_{00}b)} \quad k = m = 0 \tag{36a}$$

$$\left.\begin{aligned} C_{1km} &= \frac{\left[(-1)^{k+1}\alpha_{km} + \delta_{12} t_{2km}\right] L_{bkm} - S_{bkm}}{\sqrt{\zeta_{km}a}\mathcal{H}_j^*(t_{1km}b)\Xi_1/\mu_1} \\ C_{2km} &= -\frac{\left[(-1)^{k+1}\alpha_{km} + \delta_{11} t_{1km}\right] L_{bkm} - S_{bkm}}{\sqrt{\zeta_{km}a}\mathcal{H}_j^*(t_{2km}b)\Xi_1/\mu_1} \end{aligned}\right\} \quad \text{otherwise}, \tag{36b}$$

where $\Xi_1 = (a_1\alpha_{km}^2 - \kappa)(t_{1km}^2 - t_{2km}^2)/(t_{1km}t_{2km})$.

So far, all unknown coefficients $C_{00}, C_{1km}, C_{2km}, D_{00}, D_{1jn}$ and D_{2jn} in the general solution component of Eq. (25) have been determined using the expressions for $L_a^{kj}, L_b^{kj}, S_a^{kj}$ and S_b^{kj} in the (k,j) BC components of Eq. (32). Subsequently, an infinite system of algebraic equations is derived by substituting the above determined unknowns into the remaining entries $T_a^{kj}, T_b^{kj}, N_a^{kj}$ and N_b^{kj} in Eq. (32) and applying the modified Fourier series formula of either Eq. (B.4a) or Eq. (B.4b) to the corresponding hyperbolic functions. This infinite system can be rewritten in the following mixed-variable matrix form as:

$$\begin{bmatrix} \boldsymbol{T}^{kj} \\ \boldsymbol{N}^{kj} \end{bmatrix} = \begin{bmatrix} \boldsymbol{A}_{TL}^{kj} & \boldsymbol{A}_{TS}^{kj} \\ \boldsymbol{A}_{NL}^{kj} & \boldsymbol{A}_{NS}^{kj} \end{bmatrix} \begin{bmatrix} \boldsymbol{L}^{kj} \\ \boldsymbol{S}^{kj} \end{bmatrix} \tag{37}$$

where

$$\boldsymbol{N}^{kj} = [N_{aj0}, N_{aj1}, \ldots, N_{ajn}, \ldots, N_{bk0}, N_{bk1}, \ldots, N_{bkm}, \ldots]^T, \tag{38a}$$

$$\boldsymbol{S}^{kj} = [S_{aj0}, S_{aj1}, \ldots, S_{ajn}, \ldots, S_{bk0}, S_{bk1}, \ldots, S_{bkm}, \ldots]^T, \tag{38b}$$

$$\boldsymbol{L}^{kj} = [L_{aj0}, L_{aj1}, \ldots, L_{ajn}, \ldots, L_{bk0}, L_{bk1}, \ldots, L_{bkm}, \ldots]^T, \tag{38c}$$

$$\boldsymbol{T}^{kj} = [T_{aj0}, T_{aj1}, \ldots, T_{ajn}, \ldots, T_{bk0}, T_{bk1}, \ldots, T_{bkm}, \ldots]^T \tag{38d}$$

whose elements are the modified Fourier coefficients as given earlier in Eq. (32). It should be noted that when $j = 0, S_{aj0}$ and T_{aj0} are zero due to $\mathcal{T}_0^*(\gamma_{00}\xi) \equiv 0$ based on Eq. (B.1b). Similarly, when $k = 0, S_{bk0}$ and T_{bk0} are zero. Therefore, when $j = 0$ and/or $k = 0, S_{a00}, S_{b00}$ in Eq. (38b) and/or T_{a00}, T_{b00} in Eq.(38d) should be removed from the vectors $\boldsymbol{S}^{kj}$ and/or $\boldsymbol{T}^{kj}$, respectively. The explicit expressions of the four coefficient matrices $\boldsymbol{A}^{kj}$ in Eq. (37) are given concisely in Appendix C. Similar to the transverse vibration formulation in [55], the mixed-variable coefficient matrix of Eq. (37) also exhibits a symplectic structure: $\boldsymbol{A}_{TS}^{kj} = \boldsymbol{A}_{TS}^{kj\,T}$ and $\boldsymbol{A}_{NL}^{kj} = \boldsymbol{A}_{NL}^{kj\,T}$ are symmetric matrices, while $\boldsymbol{A}_{TL}^{kj} = -\boldsymbol{A}_{NS}^{kj\,T}$. Based on Eq. (37), the SDS matrix for each (k,j) component can be reconstructed in the following form

$$\boldsymbol{f}^{kj} = \boldsymbol{K}^{kj}\boldsymbol{d}^{kj}, \tag{39}$$

where

$$\boldsymbol{f}^{kj} = A_{66}\begin{bmatrix}\boldsymbol{N}^{kj}\\ \boldsymbol{S}^{kj}\end{bmatrix}, \quad \boldsymbol{d}^{kj} = \begin{bmatrix}\boldsymbol{L}^{kj}\\ \boldsymbol{T}^{kj}\end{bmatrix}, \tag{40}$$

$$\boldsymbol{K}^{kj} = A_{66}\begin{bmatrix}\boldsymbol{A}_{NL}^{kj} - \boldsymbol{A}_{NS}^{kj}\boldsymbol{A}_{TS}^{kj\,-1}\boldsymbol{A}_{TL}^{kj} & \boldsymbol{A}_{NS}^{kj}\boldsymbol{A}_{TS}^{kj\,-1}\\ \boldsymbol{A}_{TS}^{kj\,-1}\boldsymbol{A}_{TL}^{kj} & \boldsymbol{A}_{TS}^{kj\,-1}\end{bmatrix}. \tag{41}$$

3.2. Combing the SDS component matrices to the SDS matrix for a complete element

This section describes the combination of the four SDS component matrices ($\boldsymbol{K}^{kj}$) to form the SDS matrix of an entire element ($\boldsymbol{K}$). In essence, the relationship between $\boldsymbol{K}^{kj}$ and $\boldsymbol{K}$ is determined by that between $\boldsymbol{f}, \boldsymbol{d}$ of Eq. (30) and $\boldsymbol{f}^{kj}, \boldsymbol{d}^{kj}$ of Eq. (39). Following similar but slightly different procedure of that for transverse vibration [54], the following relationships can be reached

$$\boldsymbol{f} = \boldsymbol{T}[\boldsymbol{f}^{00\,T}, \boldsymbol{f}^{01\,T}, \boldsymbol{f}^{10\,T}, \boldsymbol{f}^{11\,T}]^T, \quad \boldsymbol{d} = \boldsymbol{T}[\boldsymbol{d}^{00\,T}, \boldsymbol{d}^{01\,T}, \boldsymbol{d}^{10\,T}, \boldsymbol{d}^{11\,T}]^T, \tag{42}$$

where $\boldsymbol{T}$ is the transfer matrix in the form

$$\boldsymbol{T} = \begin{bmatrix}
\boldsymbol{I}_n & \boldsymbol{0} & \boldsymbol{0} & \boldsymbol{0} & \boldsymbol{0} & \boldsymbol{0} & \boldsymbol{0} & \boldsymbol{0} & \boldsymbol{I}_n & \boldsymbol{0} & \boldsymbol{0} & \boldsymbol{0} & \boldsymbol{0} & \boldsymbol{0} & \boldsymbol{0} & \boldsymbol{0}\\
\boldsymbol{0} & \boldsymbol{0} & \boldsymbol{0} & \boldsymbol{0} & \boldsymbol{I}_n & \boldsymbol{0} & \boldsymbol{0} & \boldsymbol{0} & \boldsymbol{0} & \boldsymbol{0} & \boldsymbol{0} & \boldsymbol{0} & \boldsymbol{I}_n & \boldsymbol{0} & \boldsymbol{0} & \boldsymbol{0}\\
\boldsymbol{0} & \boldsymbol{0} & \boldsymbol{I}_n^{\dagger} & \boldsymbol{0} & \boldsymbol{0} & \boldsymbol{0} & \boldsymbol{0} & \boldsymbol{0} & \boldsymbol{0} & \boldsymbol{0} & \boldsymbol{I}_n^{\dagger} & \boldsymbol{0} & \boldsymbol{0} & \boldsymbol{0} & \boldsymbol{0} & \boldsymbol{0}\\
\boldsymbol{0} & \boldsymbol{0} & \boldsymbol{0} & \boldsymbol{0} & \boldsymbol{0} & \boldsymbol{0} & \boldsymbol{I}_n & \boldsymbol{0} & \boldsymbol{0} & \boldsymbol{0} & \boldsymbol{0} & \boldsymbol{0} & \boldsymbol{0} & \boldsymbol{0} & \boldsymbol{I}_n & \boldsymbol{0}\\
\boldsymbol{0} & \boldsymbol{I}_m & \boldsymbol{0} & \boldsymbol{0} & \boldsymbol{0} & \boldsymbol{I}_m & \boldsymbol{0} & \boldsymbol{0} & \boldsymbol{0} & \boldsymbol{0} & \boldsymbol{0} & \boldsymbol{0} & \boldsymbol{0} & \boldsymbol{0} & \boldsymbol{0} & \boldsymbol{0}\\
\boldsymbol{0} & \boldsymbol{0} & \boldsymbol{0} & \boldsymbol{0} & \boldsymbol{0} & \boldsymbol{0} & \boldsymbol{0} & \boldsymbol{0} & \boldsymbol{0} & \boldsymbol{I}_m & \boldsymbol{0} & \boldsymbol{0} & \boldsymbol{0} & \boldsymbol{I}_m & \boldsymbol{0} & \boldsymbol{0}\\
\boldsymbol{0} & \boldsymbol{0} & \boldsymbol{0} & \boldsymbol{I}_m^{\dagger} & \boldsymbol{0} & \boldsymbol{0} & \boldsymbol{0} & \boldsymbol{I}_m^{\dagger} & \boldsymbol{0} & \boldsymbol{0} & \boldsymbol{0} & \boldsymbol{0} & \boldsymbol{0} & \boldsymbol{0} & \boldsymbol{0} & \boldsymbol{0}\\
\boldsymbol{0} & \boldsymbol{0} & \boldsymbol{0} & \boldsymbol{0} & \boldsymbol{0} & \boldsymbol{0} & \boldsymbol{0} & \boldsymbol{0} & \boldsymbol{0} & \boldsymbol{0} & \boldsymbol{0} & \boldsymbol{I}_m & \boldsymbol{0} & \boldsymbol{0} & \boldsymbol{0} & \boldsymbol{I}_m\\
-\boldsymbol{I}_n & \boldsymbol{0} & \boldsymbol{0} & \boldsymbol{0} & \boldsymbol{0} & \boldsymbol{0} & \boldsymbol{0} & \boldsymbol{0} & \boldsymbol{I}_n & \boldsymbol{0} & \boldsymbol{0} & \boldsymbol{0} & \boldsymbol{0} & \boldsymbol{0} & \boldsymbol{0} & \boldsymbol{0}\\
\boldsymbol{0} & \boldsymbol{0} & \boldsymbol{0} & \boldsymbol{0} & -\boldsymbol{I}_n & \boldsymbol{0} & \boldsymbol{0} & \boldsymbol{0} & \boldsymbol{0} & \boldsymbol{0} & \boldsymbol{0} & \boldsymbol{0} & \boldsymbol{I}_n & \boldsymbol{0} & \boldsymbol{0} & \boldsymbol{0}\\
\boldsymbol{0} & \boldsymbol{0} & \boldsymbol{I}_n^{\dagger} & \boldsymbol{0} & \boldsymbol{0} & \boldsymbol{0} & \boldsymbol{0} & \boldsymbol{0} & \boldsymbol{0} & \boldsymbol{0} & -\boldsymbol{I}_n^{\dagger} & \boldsymbol{0} & \boldsymbol{0} & \boldsymbol{0} & \boldsymbol{0} & \boldsymbol{0}\\
\boldsymbol{0} & \boldsymbol{0} & \boldsymbol{0} & \boldsymbol{0} & \boldsymbol{0} & \boldsymbol{0} & \boldsymbol{I}_n & \boldsymbol{0} & \boldsymbol{0} & \boldsymbol{0} & \boldsymbol{0} & \boldsymbol{0} & \boldsymbol{0} & -\boldsymbol{I}_n & \boldsymbol{0}\\
\boldsymbol{0} & -\boldsymbol{I}_m & \boldsymbol{0} & \boldsymbol{0} & \boldsymbol{0} & \boldsymbol{I}_m & \boldsymbol{0} & \boldsymbol{0} & \boldsymbol{0} & \boldsymbol{0} & \boldsymbol{0} & \boldsymbol{0} & \boldsymbol{0} & \boldsymbol{0} & \boldsymbol{0} & \boldsymbol{0}\\
\boldsymbol{0} & \boldsymbol{0} & \boldsymbol{0} & \boldsymbol{0} & \boldsymbol{0} & \boldsymbol{0} & \boldsymbol{0} & \boldsymbol{0} & \boldsymbol{0} & -\boldsymbol{I}_m & \boldsymbol{0} & \boldsymbol{0} & \boldsymbol{0} & \boldsymbol{I}_m & \boldsymbol{0} & \boldsymbol{0}\\
\boldsymbol{0} & \boldsymbol{0} & \boldsymbol{0} & \boldsymbol{I}_m^{\dagger} & \boldsymbol{0} & \boldsymbol{0} & \boldsymbol{0} & -\boldsymbol{I}_m^{\dagger} & \boldsymbol{0} & \boldsymbol{0} & \boldsymbol{0} & \boldsymbol{0} & \boldsymbol{0} & \boldsymbol{0} & \boldsymbol{0} & \boldsymbol{0}\\
\boldsymbol{0} & \boldsymbol{0} & \boldsymbol{0} & \boldsymbol{0} & \boldsymbol{0} & \boldsymbol{0} & \boldsymbol{0} & \boldsymbol{0} & \boldsymbol{0} & \boldsymbol{0} & \boldsymbol{0} & \boldsymbol{I}_m & \boldsymbol{0} & \boldsymbol{0} & \boldsymbol{0} & -\boldsymbol{I}_m
\end{bmatrix}, \tag{43}$$

and in which $\boldsymbol{I}_n, \boldsymbol{I}_n^{\dagger}, \boldsymbol{I}_m$ and $\boldsymbol{I}_m^{\dagger}$ are identity matrices of dimension $n, n-1, m$ and $m-1$ respectively, and $\boldsymbol{0}$ represents null matrices. Also, it is found that $\boldsymbol{T}^{-1} = \boldsymbol{T}^T/2$; therefore, the second equation of Eq. (42) will lead to

$$[\boldsymbol{d}^{00\,T}, \boldsymbol{d}^{01\,T}, \boldsymbol{d}^{10\,T}, \boldsymbol{d}^{11\,T}]^T = \frac{1}{2}\boldsymbol{T}^T\boldsymbol{d}. \tag{44}$$

Finally, putting Eqs. (39), (30), (42) and (44) together yields

$$\boldsymbol{f} = \boldsymbol{K}\boldsymbol{d}, \tag{45}$$

where

$$\boldsymbol{K} = \frac{1}{2}\boldsymbol{T}\begin{bmatrix}\boldsymbol{K}^{00} & \boldsymbol{0} & \boldsymbol{0} & \boldsymbol{0}\\ \boldsymbol{0} & \boldsymbol{K}^{01} & \boldsymbol{0} & \boldsymbol{0}\\ \boldsymbol{0} & \boldsymbol{0} & \boldsymbol{K}^{10} & \boldsymbol{0}\\ \boldsymbol{0} & \boldsymbol{0} & \boldsymbol{0} & \boldsymbol{K}^{11}\end{bmatrix}\boldsymbol{T}^T \tag{46}$$

is the SDS matrix for the inplane vibration of the entire element.

3.3. Assembly procedure and the application of arbitrary classical BCs

The SDS matrices for all elements can be assembled directly to form the global SDS matrix of the complete structure. The procedure follows that described in [55], which will not be repeated here. Any classical boundary conditions can then be applied onto the global SDS matrix by condensing all DOFs relating to all fixed line nodes. It is worth emphasising that the condensing procedure is in an exact sense and there is no penalty method involved here in the SDSM like other methods [39,3,47,48]. So there is no need to determine a sufficient 'large parameter' to model fixed DOFs and therefore, completely avoiding the possible modelling errors or numerical instability due to an improperly chosen penalty

parameter [49]. The treatment of more general non-classical boundary conditions are given in the next section.

4. The SDS formulation for non-uniform elastic supports, mass attachments and coupling constraints for inplane vibration

The general SDS theory dealing with arbitrary non-uniform elastic supports, mass attachments and coupling constraints are described in [58] with the basic premise that the Kirchhoff plate theory is applied. However, some extra attention should be paid when applying the general SDS theory [58] to the current inplane vibration problems, which is therefore briefly described as follows.

According to the theory given in [58], the additional force $f_i^a(\xi)$ resulting from an arbitrary non-uniform elastic support or mass attachment applied along the ith line node ($\xi \in [-L, L]$) can be described by the following expression

$$f_i^a(\xi) = \mu G^a(\xi) d_i(\xi), \quad \xi \in [-L, L]. \tag{47}$$

Similarly, the additional forces $f_i^a(\xi)$ and $f_j^a(\xi)$ generated by an arbitrary non-uniform elastic coupling constraint applied between the ith and jth line nodes (both with matching edges $\xi \in [-L, L]$) can be expressed in the form

$$\begin{bmatrix} f_i^a(\xi) \\ f_j^a(\xi) \end{bmatrix} = \mu \begin{bmatrix} G^a(\xi) & -G^a(\xi) \\ -G^a(\xi) & G^a(\xi) \end{bmatrix} \begin{bmatrix} d_i(\xi) \\ d_j(\xi) \end{bmatrix}, \quad \xi \in [-L, L]. \tag{48}$$

In the current inplane vibration problem, $f_i^a(\xi)$ in Eqs. (47) and (48) (also applies to $f_j^a(\xi)$) represents either additional normal N_i^a or shear S_i^a forces along the ith line node $\xi \in [-L, L]$ resulting from the additional elastic supports, mass attachments or coupling constraints; whereas $d_i(\xi)$ denotes either the normal L_i or tangent T_i displacement accordingly. Also in Eqs. (47) and (48), $G^a(\xi)$ is a *dimensionless distribution function* and μ is the *stiffness* or *mass dynamic stiffness constant* which represents one of the three constants: K_{L0}, K_{T0} or $-\omega^2 m_0$. In particular, for the inplane vibration of plates with the plane stress reduced stiffnesses given in Eq. (16), both K_{L0} and K_{T0} have the same dimension of $[\widehat{M}][\widehat{L}]^{-1}[\widehat{T}]^{-2}$ with the corresponding dimensionless forms $K_{L0}L_b/A_{66}$ and $K_{T0}L_b/A_{66}$ respectively. ($[\widehat{M}], [\widehat{L}]$ and $[\widehat{T}]$ stand for mass, length and time respectively in the dimension analysis, and L_b denotes the length of the line nodes, i.e., $2L$). Also, m_0 has the dimension of $[\widehat{M}][\widehat{L}]^{-1}$ with the dimensionless form $m_0 L_b/m_p$, where m_p is the total mass of the parent structure. It is understandable that for inplane vibration of prismatic solids with the reduced stiffnesses and inertia given in Eq. (17), the dimensions of K_{L0}, K_{T0} and m_0 can be obtained by dividing their dimensions in the plane stress case by the dimension of plate thickness ($[\widehat{L}]$). The application of the non-uniform elastic support or mass attachment described by Eq. (47) along the ith line node is performed easily by

$$\boldsymbol{K}_{ii}^{final} = \boldsymbol{K}_{ii} + \mu \boldsymbol{G}^a, \tag{49}$$

which means that the ii component of the final SDS matrix ($\boldsymbol{K}_{ii}^{final}$) will have the additional contribution from the elastic support or mass attachment. Similarly, the ii, ij, ji and jj components of the final SDS matrices will incorporate the additional contributions resulting from the elastic coupling constraint of Eq. (48), hence

$$\begin{aligned} \boldsymbol{K}_{ii}^{final} &= \boldsymbol{K}_{ii} + \mu \boldsymbol{G}^a, \quad \boldsymbol{K}_{jj}^{final} = \boldsymbol{K}_{jj} + \mu \boldsymbol{G}^a, \\ \boldsymbol{K}_{ij}^{final} &= \boldsymbol{K}_{ij} - \mu \boldsymbol{G}^a, \quad \boldsymbol{K}_{ji}^{final} = \boldsymbol{K}_{ji} - \mu \boldsymbol{G}^a. \end{aligned} \tag{50}$$

In both Eqs. (49) and (50), $\boldsymbol{G}^a$ is the *dimensionless SDS matrix* corresponding to the dimensionless distribution function $G^a(\xi)$ in Eqs. (47) and (48). It should be noted that the formulation of $\boldsymbol{G}^a$ is in a very accurate yet versatile fashion. If the distribution function $G^a(\xi)$ can be written as the linear combination of some known functions, the corresponding $\boldsymbol{G}^a$ matrix is simply the linear combination of the $\boldsymbol{G}^a$ matrices of these known functions. Besides, any $\boldsymbol{G}^a$ matrix should be a symmetric matrix that can be generally expressed in the following form

$$\boldsymbol{G}^a = \begin{bmatrix} \boldsymbol{G}_{00}^a & \boldsymbol{G}_{01}^a \\ \boldsymbol{G}_{10}^a & \boldsymbol{G}_{11}^a \end{bmatrix}. \tag{51}$$

Here special attention should be paid in the formulation of the above four $\boldsymbol{G}_{tl}^a$ (with $t, l \in \{0, 1\}$) matrices for the current inplane vibration case.

When the $f_i^a(\xi)$ and $d_i(\xi)$ in Eq. (47) or (48) represent respectively the normal stress N_i and displacement L_i, the formulation of the $\boldsymbol{G}_{tl}^a$ matrices will follow exactly the procedure given in [58]. In that way, the analytical expressions for $\boldsymbol{G}_{tl}^a$ can be obtained from the following equation by using the first type of modified Fourier series (B.2), i.e.,

$$\boldsymbol{G}_{tl}^a(r, s) = \frac{1}{\sqrt{\zeta_{tr}\zeta_{ls}}L} \int_{-L}^{L} G^a(\xi) \mathcal{T}_l(\gamma_{ls}\xi) \mathcal{T}_t(\gamma_{tr}\xi) \mathrm{d}\xi. \tag{52}$$

In such a case, all four matrices $\boldsymbol{G}_{tl}^a$ are $S \times S$ matrices if S terms are adopted in the modified Fourier series, namely, $s, r \in [0, S-1]$. (Here, S coincides with M or N where M and N are the numbers of terms adopted in the series for the related element in the x and y directions respectively.) The $\boldsymbol{G}_{tl}^a$ matrices obtained by using Eq. (52) for some typical distribution functions have already been given in Appendix A of [58]. However, when $f_i^a(\xi)$ and $d_i(\xi)$ in Eq. (47) or (48) represent respectively the tangent stress S_i and displacement T_i, the formulation of the $\boldsymbol{G}_{tl}^a$ matrices will be slightly different by applying the second type of modified Fourier series (B.3) to give

$$\boldsymbol{G}_{tl}^a(r, s) = \frac{1}{\sqrt{\zeta_{tr}\zeta_{ls}}L} \int_{-L}^{L} G^a(\xi) \mathcal{T}_l^*(\gamma_{ls}\xi) \mathcal{T}_t^*(\gamma_{tr}\xi) \mathrm{d}\xi. \tag{53}$$

In this case, if S terms are adopted in the modified Fourier series, the size of four sub-matrices $\boldsymbol{G}_{00}^a, \boldsymbol{G}_{01}^a, \boldsymbol{G}_{10}^a$ and $\boldsymbol{G}_{11}^a$ will be $(S-1)\times(S-1), (S-1)\times S, S\times(S-1)$ and $S\times S$, respectively. The analytical expressions for the $\boldsymbol{G}_{tl}^a$ matrices for some typical distribution functions derived from Eq. (53) are given in Appendix D of this paper.

5. The Wittrick-Williams algorithm and its enhancement

In order to compute the natural frequencies of a structure using the SDSM, the most reliable and efficient solution technique is probably the Wittrick-Williams (WW) algorithm [60]. However, some difficulties may arise in the WW algorithm application, but for the current problem all potential stumbling blocks have been removed so as to make the current SDSM reliable, computationally efficient and accurate within the whole frequency range. For clarity and completeness, the procedure is briefly summarised as follows. Suppose that the overall SDS matrix of the final structure is denoted by $\boldsymbol{K}_f$, which is a transcendental matrix function of circular frequency ω. Then according to the WW algorithm, as ω increases from zero to ω^*, the number of natural frequencies of the final structure passed (mode count J) is given by

$$J = J_0 + s\{\boldsymbol{K}_f^*\}, \tag{54}$$

where $s\{\boldsymbol{K}_f^*\}$ corresponds to the negative inertia of the $\boldsymbol{K}_f^*$ according to Sylvester's law [61], and $\boldsymbol{K}_f^*$ represents $\boldsymbol{K}_f$ when $\omega = \omega^*$. The above $s\{\boldsymbol{K}_f^*\}$ can be computed by applying the usual form of Gauss elimination to $\boldsymbol{K}_f$ leading to a upper triangular matrix, and then

$s\{\boldsymbol{K}_f^*\}$ is the number of negative elements on the leading diagonal of the upper triangular matrix. Meanwhile, the J_0 of Eq. (54) is given by

$$J_0 = \sum_m J_{0m}, \tag{55}$$

where $J_{0m}$is the number of natural frequencies between $\omega = 0$ and $\omega = \omega^*$ for an individual component member with its boundaries fully clamped, while the summation extends over all structural members. Thus, with the knowledge of Eqs. (54) and (55), one can compute any natural frequency up to the desired accuracy by using bracket methods such as bi-section technique.

It is clear from above that the J_{0m} count is an essential part of the algorithm. However, it is well-known that the computation of J_{0m} count can sometimes be a difficult task and may become a potential drawback when applying the WW algorithm. In the literature, most of the previous DS methods [3–5,34] used a sufficiently fine mesh to avoid J_{0m} computation i.e., to ensure that $J_{0m} \equiv 0$ for the entire frequency range of interest. However, this will no doubt increase the computational time. This is particularly true for the current SDSM because a finer mesh will increase the number of DOF much more significantly than the classical DSM. (Also, substructuring technique becomes less attractive in this case due to the same reason.) To meet this challenge, an efficient and reliable strategy is applied which is based on the closed-form solution of each member subject to all-round simple supports. Obviously, Eq. (54) also applies for such a special case for each member, i.e., $J_{Sm} = J_{0m} + s\{\boldsymbol{K}_{Sm}^*\}$, where J_{Sm} is the mode count of a certain member with all boundaries simply supported, and $s(\boldsymbol{K}_{Sm}^*)$ is the sign count of its formulated SDS matrix $\boldsymbol{K}_{Sm}$ when $\omega = \omega^*$. Therefore, J_{0m} of Eq. (55) is given by

$$J_{0m} = J_{Sm} - s(\boldsymbol{K}_{Sm}^*), \tag{56}$$

where both J_{Sm} and $s(\boldsymbol{K}_{Sm}^*)$ are computed efficiently and elegantly in this paper as described as follows. First, the J_{Sm} of Eq. (56) is obtained analytically by solving a Number Theory problem. It is known that the closed-form exact solution for the natural frequencies of an all-round simply supported (S_2) orthotropic plate (also applies for plane strain cases) is given in Eq. (32) of Ref. [38] by Liu and Xing, which can be rewritten in the following dimensionless form

$$\frac{2\rho}{A_{66}}\left(\frac{2a\omega_{\hat{m}\hat{n}}}{\pi}\right)^2 = \Pi_A - \Pi_B, \quad \hat{m},\hat{n} \in \{1,2,3,\ldots\} \tag{57}$$

$$\frac{2\rho}{A_{66}}\left(\frac{2a\omega_{\hat{m}\hat{n}}}{\pi}\right)^2 = \Pi_A + \Pi_B, \quad \hat{m},\hat{n} \in \{0,1,2,3,\ldots\} \text{ except } \hat{m} = \hat{n} = 0. \tag{58}$$

In Eqs. (57) and (58), $\omega_{\hat{m}\hat{n}}$ is the natural circular frequency with $\hat{m}$ and $\hat{n}$ being the half-wave numbers in the x and y direction respectively, and

$$\Pi_A = (a_1+1)\hat{m}^2 + (a_2+1)(\eta\hat{n})^2, \quad \eta = a/b,$$
$$\Pi_B = \sqrt{\left[(a_1-1)\hat{m}^2 - (a_2-1)(\eta\hat{n})^2\right]^2 + 4(a_3+1)^2\hat{m}^2(\eta\hat{n})^2}$$

Thus, J_{Sm}, the number of natural frequencies lying below a trial frequency ω^*, is essentially the total number of combinations of $(\hat{m},\hat{n})$ such that the left-hand sides of Eqs. (57) and (58) with $\omega_{\hat{m}\hat{n}} = \omega^*$ are no less than the right-hand sides, respectively. Therefore,

$$J_{Sm} = J_{Sm1} + J_{Sm2}, \tag{59}$$

where J_{Sm1} and J_{Sm2} are respectively the contributions from Eqs. (57) and (58). Obviously, J_{Sm1} and J_{Sm2} can be obtained from a numerical search which may be computationally expensive and the procedure may miss some of the natural frequencies. However, there exists an analytical expression for J_{Sm1} and J_{Sm1} and this problem is essentially an extension of the *Gauss circle problem* [62] in the field of Analytical Number Theory. The expressions for J_{Sm1} and J_{Sm2} can be deduced by solving the inequalities for which the left-hand sides of Eqs. (57) and (58) with $\omega_{\hat{m}\hat{n}} = \omega^*$ are no less than the right-hand sides, hence

$$J_{Sm1} = \sum_{\hat{m}=1}^{\lfloor\Pi_2\rfloor}\left\lfloor\sqrt{\Pi_4 + \sqrt{\Pi_4^2 - \Pi_5}}/(2\eta\sqrt{a_2})\right\rfloor, \tag{60}$$

$$J_{Sm2} = \sum_{\hat{m}=0}^{\lfloor\Pi_3\rfloor}\left\lfloor\sqrt{\Pi_4 - \sqrt{\Pi_4^2 - \Pi_5}}/(2\eta\sqrt{a_2}) + \text{sign}(\hat{m})\right\rfloor, \tag{61}$$

where '$\lfloor\cdot\rfloor$' is the floor function denoting the largest integer not greater than '$\cdot$' and

$$\Pi_2 = \sqrt{\frac{\Pi_6 + \sqrt{\Pi_6^2 - \Pi_7}}{4a_1}}, \quad \Pi_3 = \sqrt{\frac{\Pi_1}{(a_1+1) + |a_1-1|}},$$
$$\Pi_1 = \left(\frac{2a}{\pi}\right)^2\frac{2\rho\omega^{*2}}{A_{66}},$$
$$\Pi_4 = 2[a_3(a_3+2) - a_1a_2]\hat{m}^2 + (a_2+1)\Pi_1,$$
$$\Pi_5 = 4a_2(2\hat{m}^2 - \Pi_1)(2a_1\hat{m}^2 - \Pi_1),$$
$$\Pi_6 = \Pi_1(a_1+1) + 2[a_3(a_3+2) - a_1a_2]\eta^2,$$
$$\Pi_7 = 4a_1(\Pi_1 - 2\eta^2)(\Pi_1 - 2a_2\eta^2).$$

Next, the $s(\boldsymbol{K}_{Sm}^*)$ of Eq. (56) is computed in an elegant way by taking advantage of the mixed-variable formulation of the (k,j) symmetric/antisymmetric components explained earlier in Section 3.1. It is well-known that when a symmetric structure is subject to symmetric constraints, the displacement field will be either symmetric or antisymmetric. Therefore, in the present case where a rectangular element is subjected to all round simple supports, any possible natural mode can be described by one of the four symmetric/antisymmetric SDS matrices. In this case, $s(\boldsymbol{K}_{Sm}^*) = \sum_{k,j\in\{0,1\}} s(\boldsymbol{K}_{Sm}^{kj\,*})$. Now recalling Eqs. (39)–(41), the case with fully simple supports of type S_2 becomes equivalent to letting $\boldsymbol{L}^{kj} = \boldsymbol{S}^{kj} = \boldsymbol{0}$, such that $s(\boldsymbol{K}_{Sm}^{kj\,*}) = s(\boldsymbol{A}_{TS}^{kj\,*^{-1}})$. In this way, one has

$$s(\boldsymbol{K}_{Sm}^*) = \sum_{k,j\in\{0,1\}} s(\boldsymbol{A}_{TS}^{kj\,*^{-1}}) = \sum_{k,j\in\{0,1\}} s(\boldsymbol{A}_{TS}^{kj\,*}). \tag{62}$$

The above techniques given in Eqs. (56)–(62) have completely resolved the previous J_0 count problem of Eq. (55) in a highly efficient, accurate and reliable manner within the whole frequency range.

After obtaining the natural frequencies, the corresponding mode shapes are computed using the global SDS matrix $\boldsymbol{K}_f$ in a similar procedure as described in [55]. However, in the inplane mode shape computation, the mode shape should be normalised by using a carefully chosen DOF which causes the sign count of $\boldsymbol{K}_f$ to increase when applying the Wittrick-Williams algorithm. This is similar to the DSM for Levy-type plate [3].

6. Modelling procedure of the spectral dynamic stiffness method

To assist the interested readers to use the proposed method easily, we detail the modelling procedure of the spectral dynamic stiffness (SDS) method as following:

(i) Partitioning the domain of the considered problem into elements;

(ii) Evaluating the elemental SDS matrices $\boldsymbol{K}$ and calculating the J_{0m} count at a trial frequency ω^* for each element, this includes
(a) Evaluating the material constants for each element by using Eq. (15), with Eqs. (16) and (A.5) for plane stress and Eqs. (17) and (A.7) for plane strain.
(b) Evaluating the four $\boldsymbol{A}_{..}^{kj}$ matrices of Eq. (C.1) in the mixed-variable formulation for each (k,j) component, where the wavenumber related coefficients $\alpha_{km}, \beta_{jn}, r_{ijn}$ and t_{ikm} are defined in (18), (21) and (27), whereas ζ_{km} and ζ_{jn} are defined in Eq. (B.1); Computing $s(\boldsymbol{A}_{TS}^{kj})$ of Eq. (62) for each (k,j) component.
(c) Calculating the four SDS component matrices $\boldsymbol{K}^{kj}$ by using Eq. (41) and combining them to the SDS matrix $\boldsymbol{K}$ for a complete element by using Eq. (46); Computing J_{0m} for each element through Eqs. (56), (59) and (62).
(iii) Assembling all elemental SDS matrices for the considered structure and applying any arbitrarily prescribed classical BCs following the procedure described in Section 3.3; Computing J_0 count for the global structure by using Eq. (55).
(iv) Applying any arbitrarily prescribed non-classical BCs by using Eqs. (49) and/or (50), where the general $\boldsymbol{G}^a$ matrices are given in Eq. (51) by applying Eqs. (52) and (53) to any arbitrarily given distribution function.
(v) Computing natural frequencies using the Wittrick-Williams algorithm of Eq. (54); obtaining mode shapes following the procedure described in the last paragraph of Section 5.

7. Results and discussion

The theory described in this paper is implemented in a `Matlab` code using objected-oriented programming technique, which is very easy to use and open for further development. The SDSM has been previously developed for transverse vibration of isotropic plates [54] and complex composite plate assemblies [55,58], which has been demonstrated to give exact results very efficiently, covering both low and medium to high frequency ranges. Moreover, the method has unconditionally computational stability, allowing the computation of results up to any required precision. In this section, it will be shown that the above advantages remain in the SDSM for free inplane vibration. In Section 7.1, the excellent convergence rate and numerical efficiency of the proposed method will first be demonstrated, then the SDSM results are validated against published results wherever available and applied for some other representative cases. In Sections 7.2 and 7.3, the SDSM is applied for the inplane modal analysis of several wide-ranging engineering problems.

7.1. Convergence and numerical efficiency studies and validation

The first case to be analysed is the free inplane vibration of a fully clamped orthotropic plate. This case has been chosen in most of the existing work [33,39,47,48] on free inplane vibration of orthotropic plates, allowing the comparison analysis given in Table 1. All of the SDSM results were computed on a PC with a 3.40 GHz Intel 4-core processor and 8 GB of memory. The number of terms included in the series (or elements) for each method are shown in the third column in the form of (M,N); the accuracy (in terms of Sig. Dig., i.e., significant digits) and computation time are tabulated in the last two columns whenever available. Note that $M+N$ means the final matrix size is proportional to the summation of M and N whereas $M \times N$ indicated that the final matrix size is proportional to their product instead.

Indeed, the proposed SDSM exhibits an very fast convergence rate. As evident from Table 1, only five (ten/fifteen) series terms adopted in the SDSM lead to results with accuracy of at least four (five/six) significant digits. In comparison, the two Ritz methods (Ritz(IFS) [48] and Ritz(trig.) [39]) used 14 and 18 terms respectively in the series leading to results with five significant digit precision; the Fourier series based analytical methods (FSA) [47] used 12 terms but gave results with accuracy of only three significant figures. The Gorman's superposition method (GSM) [33] on the other hand, gave results with four digit precision using 9 terms in the series. More importantly, the number of DOFs involved in the SDSM is proportional to $M+N$, which is in a sharp contrast to other methods (except the GSM [33]) whose numbers of DOFs are proportional to $M \times N$. For example, to compute results with five significant digits, the total number of DOFs involved in the

Table 1
Dimensionless frequency parameter $\lambda = \omega a\sqrt{\rho(1-\nu_{12}\nu_{21})/E_1}$ for free inplane vibration of fully clamped orthotropic plates ($E_2/E_1 = 2.5, \nu_{12}\nu_{21} = 0.3^2, G_{12} = \sqrt{E_1E_2}/[2(1+\sqrt{\nu_{12}\nu_{21}})]$) with two different aspect ratios: $b/a = 0.5$ and 2. It should be noted that

b/a	Method	M,N	1	2	3	4	5	6	7	8	Sig. Dig.	Time(s)
0.5	SDSM	3 + 3	2.78292	3.81369	4.66319	4.77783	5.06754	5.24816	5.26108	5.96234	3	0.10
		5 + 5	2.78300	3.81404	4.66348	**4.77815**	5.06812	5.24827	5.26527	5.96743	4	0.13
		10 + 10	**2.78303**	3.81416	**4.66350**	**4.77815**	5.06829	5.24830	5.26553	5.96783	5	0.15
		15 + 15	**2.78303**	**3.81418**	**4.66350**	**4.77815**	**5.06832**	**5.24832**	**5.26554**	**5.96786**	6	0.16
		20 + 20	**2.78303**	**3.81418**	**4.66350**	**4.77815**	**5.06832**	**5.24832**	**5.26554**	**5.96786**	6	0.17
	Ritz(IFS)[48]	14 × 14	2.7830	3.8142	4.6635	4.7781	5.0683	5.2483	5.2655	5.9678	5	6.20
	Ritz(trig.)[39]	18 × 18	2.7830	3.8142	4.6635	4.7782	5.0683	5.2484	5.2656	5.9679	5	–
	FSA[47]	12 × 12	2.7830	3.8152	4.6647	4.7787	5.0704	5.2496	5.2660	5.9707	3	–
	GSM[33]	9 + 9	–	3.814	4.663	4.778	–	5.240	5.266	5.964	4	–
	FEM[48]	100 × 50	2.7828	3.1834	4.6633	4.7771	5.0621	5.2469	5.2644	5.9665	3	79.5
2	SDSM	3 + 3	1.63843	1.66709	1.83352	2.19163	2.56529	2.57581	2.7254	3.03389	4	0.10
		5 + 5	1.63851	1.66718	1.83367	2.19251	2.56586	**2.57599**	2.72611	3.03392	5	0.13
		10 + 10	**1.63853**	**1.66720**	**1.83370**	2.19257	2.56594	**2.57599**	2.72621	**3.03393**	5	0.15
		15 + 15	**1.63853**	**1.66720**	**1.83370**	**2.19258**	**2.56595**	**2.57599**	**2.72622**	**3.03393**	6	0.16
		20 + 20	**1.63853**	**1.66720**	**1.83370**	**2.19258**	**2.56595**	**2.57599**	**2.72622**	**3.03393**	6	0.17
	Ritz(IFS)[48]	14 × 14	1.6385	1.6672	1.8337	2.1926	2.566	2.576	2.7262	3.0339	5	6.20
	Ritz(trig.)[39]	18 × 18	1.6385	1.6672	1.8337	2.1926	2.566	2.576	2.7262	3.0339	5	–
	FSA[47]	12 × 12	1.6386	1.6673	1.8341	2.1934	2.5669	2.5777	2.7281	3.0352	3	–
	GSM[33]	9 + 9	–	1.667	–	–	2.566	2.576	2.7262	3.034	4	
	FEM[48]	50 × 100	1.6382	1.6663	1.8326	2.1912	2.5653	2.5745	2.7249	3.0315	3	79.5

Ritz(IFS) – Ritz method based on Improved Fourier Series [48].
Ritz(trig.) – Ritz method based on trigonometric functions [39].
FSA – Fourier series based analytical method [47].
GSM – Gorman's superposition method[33].

SDSM is only 79 (when $M+N=10+10$), whereas the Ritz (IFS) method [48] needed 570 DOFs ($M\times N=14\times 14$). The FEM [48] on the other hand, used as much as 10,201 DOFs (50×100 elements) but led to results with only three-significant-digit accuracy. Indeed, the SDSM represents the dynamic system very accurately by using a much smaller number of DOFs compared to other methods. As a result, it is to be expected that the SDSM is much more efficient than other methods. For example, as evident from Table 1, the SDSM provided more accurate results by taking only 2% and 0.2% of the computation time taken by the Ritz(IFS) method [48] and FEM [48] respectively (the computation of the two latter methods [48] were conducted on a more advanced hardware with Intel i7 3.9 GHz). The superiority of the SDSM over other methods will be more significant for higher frequencies, which has been shown for the transverse free vibration of composite plates [56] and plane elastodynamic problems [57] and will not be shown here for brevity. In the remainder of this paper, all SDSM results will be shown in bold to indicate that the SDSM results are accurate up to the last digit quoted for benchmark purposes.

After showing the computational performance of the SDSM, now we validate the SDSM for orthotropic plates with classical BCs which have closed-form exact solutions available [38] to illustrate the high accuracy of the SDSM results. Twelve cases are considered and shown in Table 2. The four sequential letters denote respectively the boundary conditions along the right, up, left and bottom plate edges in an anticlockwise sense. The letters 'C' and 'F' represent clamped and free edges whereas 'S_1' and 'S_2' stand for edges with $T=0, N=0$ and $L=0, S=0$ respectively. In Table 2, exact results are computed by the SDSM for the 12 cases with accuracy of six significant figures, the first five figures of which all coincide with the closed-form exact solutions [38] presented with five significant figures. It should be noted that in the both cases $S_2S_1S_2F$ and S_2FS_2F, the fundamental natural frequency should be zero corresponding to rigid body modes. It is worth highlighting that rigid modes are not trivial in certain analyses (e.g., for remote components, rotating shafts, lying aircraft, satellites). So it is very important that the algorithm can automatically detect their presence to spot potential mechanisms. In the present SDSM, the rigid modes are captured without any miss due to the application of the Wittrick-William algorithm.

Now we are in position to apply the present method to the free inplane vibration of orthotropic plates with other classical BCs where closed-form exact solution is not available. Table 3 tabulates the dimensionless natural frequency parameters for orthotropic plates with two aspect ratios ($a/b=1$ and 2) and subjected to eight different classical BCs. All results are presented with accuracy of five significant figures for further comparison purposes, which are compared with finite element solutions.

After shown the application of the current SDSM to plates with classical BCs, now we apply the SDSM to the free inplane vibration of plates with non-uniform elastic supports. As the only few existing work [46–48] have been confined to free inplane vibration of plates with uniform elastic supports, the sole existing contribution dealing with non-uniform inplane elastic supports appears to be made by Dozio [43], which was applied to individual isotropic plates. (It should be kept in mind that the current SDSM method treats non-uniform elastic supports in a very concise and accurate manner, in which the SDS matrices of those elastic supports are superposed directly to the global SDS matrix of the complete structure in a strong form.) Table 4 shows the first ten inplane natural frequencies of a square plate with identical elastic supports along all four edges. Both normal (L) and tangent (T) directions have the same stiffness distribution, being either triangular ($E_{\hat{L}\hat{T}}$) or parabolic ($E_{\breve{L}\breve{T}}$). Note that E stands for an elastic support; and the subscripts L and T denote normal and tangent displacements respectively; the stiffness distributions of these elastic supports are indicated by putting a corresponding accent over the subscripts L and T, where $\bar{(\,)}, \hat{(\,)}, \breve{(\,)}$ and $\grave{(\,)}$ stand for uniform, triangular, parabolic and V-shaped distributions respectively, with the corresponding dimensionless distribution functions $G^a(\xi)$ taking the form

$$\bar{(\,)}: G^a(\xi)=1, \qquad \breve{(\,)}: G^a(\xi)=1-(\xi/L)^2, \tag{63a}$$

$$\hat{(\,)}: G^a(\xi)=1-|\xi/L|, \quad \grave{(\,)}: G^a(\xi)=|\xi/L|, \tag{63b}$$

Table 2
Dimensionless frequency parameters $\lambda=(2a)\omega/\pi\sqrt{\rho/G_{xy}}$ for a square orthotropic plate ($E_1/E_2=2, \nu_{12}=0.3, A_{22}/A_{66}=2$) with twelve classical BCs. The results computed by the present method are compared with closed-form exact solutions by Liu and Xing [38].

BCs	Method	1	2	3	4	5	6	7	8	9	10
$S_2S_1S_2C$	**SDSM**	**0.707107**	**1.16188**	**1.91769**	**2.07792**	**2.12132**	**2.37894**	**2.60524**	**2.81997**	**3.05076**	**3.27893**
	Exact [38]	0.7071	1.1619	1.9177	2.0779	2.1213	2.3789	2.6052	2.8200	3.0508	3.2789
$S_2S_2S_2C$	**SDSM**	**1.41421**	**1.52284**	**2.08147**	**2.29316**	**2.34934**	**2.80605**	**2.82843**	**2.97501**	**3.19746**	**3.34724**
	Exact [38]	1.4142	1.5228	2.0815	2.2932	2.3493	2.8060	2.8284	2.3975	3.1975	3.3472
S_2CS_2C	**SDSM**	**1.41421**	**1.61731**	**2.12219**	**2.32376**	**2.78530**	**2.82843**	**2.85223**	**3.04568**	**3.21157**	**3.68659**
	Exact [38]	1.4142	1.6173	2.1222	2.3238	2.7853	2.8284	2.8522	3.0457	3.2116	3.6866
$S_2S_1S_2F$	**SDSM**	**0**	**0.895708**	**1.41421**	**1.43242**	**1.85173**	**2.07201**	**2.18177**	**2.34173**	**2.78930**	**2.81577**
	Exact [38]	–	0.8957	1.4142	1.4324	1.8517	2.0720	2.1818	2.3417	2.7893	2.8158
$S_2S_2S_2F$	**SDSM**	**0.707107**	**1.00610**	**1.84694**	**1.87161**	**2.01824**	**2.12132**	**2.38582**	**2.50525**	**2.79272**	**2.80943**
	Exact [38]	0.7071	1.0061	1.8469	1.8716	2.0182	2.1213	2.3858	2.5053	2.7927	2.8094
S_2CS_2F	**SDSM**	**0.707107**	**1.03010**	**1.87465**	**1.87683**	**2.12132**	**2.27309**	**2.42792**	**2.55767**	**2.79317**	**3.23387**
	Exact [38]	0.7071	1.0301	1.8746	1.8768	2.1213	2.2731	2.4279	2.5577	2.7932	3.2339
S_2FS_2F	**SDSM**	**0**	**0.805897**	**1.39655**	**1.41421**	**1.79142**	**2.01219**	**2.01457**	**2.11312**	**2.75428**	**2.79478**
	Exact [38]	–	0.8059	1.3965	1.4142	1.7914	2.0122	2.0146	2.1131	2.7543	2.7948
$S_2S_1S_1C$	**SDSM**	**0.808655**	**1.39265**	**1.60578**	**2.00191**	**2.24882**	**2.38088**	**2.56151**	**3.00158**	**3.02199**	**3.05274**
	Exact [38]	0.8087	1.3927	1.6058	2.0019	2.2488	2.3809	2.5615	3.0016	3.0220	3.0527
$S_2S_2S_1C$	**SDSM**	**1.06110**	**1.42612**	**1.84329**	**1.88106**	**2.54023**	**2.64823**	**2.73644**	**2.99418**	**3.07203**	**3.33072**
	Exact [38]	1.0611	1.4261	1.8433	1.8811	2.5402	2.6482	2.7364	2.9942	3.0720	3.3307
S_2CS_1C	**SDSM**	**1.38640**	**1.44263**	**1.93149**	**2.24522**	**2.70359**	**2.75658**	**2.76478**	**3.24250**	**3.32864**	**3.38105**
	Exact [38]	1.3864	1.4426	1.9315	2.2452	2.7036	2.7566	2.7648	3.2425	3.3286	3.3810
$S_2S_1S_1F$	**SDSM**	**0.402948**	**1.05656**	**1.37714**	**1.39739**	**1.77269**	**1.86286**	**2.32182**	**2.53195**	**2.57525**	**2.62884**
	Exact [38]	0.4029	1.0566	1.3771	1.3974	1.7727	1.8629	2.3218	2.3520	2.5735	2.6288
$S_2S_2S_1F$	**SDSM**	**0.698274**	**1.00728**	**1.41264**	**1.42337**	**1.98215**	**2.16028**	**2.33020**	**2.39275**	**2.89676**	**2.93652**
	Exact [38]	0.6983	1.0073	1.4126	1.4234	1.9822	2.1603	2.3302	2.3928	2.8968	2.9365

Table 3
The first ten dimensionless frequency parameters $\lambda = (2a)\omega/\pi\sqrt{\rho/G_{xy}}$ for a rectangular orthotropic plate ($E_1/E_2 = 2, \nu_{12} = 0.3, A_{22}/A_{66} = 2$) with two aspect ratios and subjected to eight different classical BCs where closed-form exact solution is not available. The SDSM results are compared with results computed by ANSYS using a 100×100 mesh ($a/b = 1$) or a 200×100 ($a/b = 2$) mesh of Plane 182 elements.

BCs	a/b	1	2	3	4	5	6	7	8	9	10
FFFF	1	**0**	**0**	**0**	**1.1761**	**1.2455**	**1.3568**	**1.4961**	**1.6268**	**1.9987**	**2.0164**
	(FEM)	0	0	0	1.1762	1.2457	1.3569	1.4964	1.6270	1.9992	2.0164
	2	**0**	**0**	**0**	**1.2097**	**1.8295**	**1.9204**	**2.5693**	**2.6025**	**2.6273**	**2.7380**
	(FEM)	0	0	0	1.2097	1.8296	1.9204	2.5696	2.6027	2.6277	2.7382
CFFF	1	**0.36944**	**0.97671**	**1.0012**	**1.3419**	**1.5115**	**1.5943**	**2.1492**	**2.1949**	**2.4509**	**2.5575**
	(FEM)	0.36948	0.97674	1.0013	1.3420	1.5117	1.5946	2.1500	2.1956	2.4518	2.5584
	2	**0.25747**	**0.92410**	**0.97887**	**1.8989**	**2.3550**	**2.5902**	**2.6392**	**2.9788**	**3.0841**	**3.1183**
	(FEM)	0.25749	0.92416	0.97888	1.8992	2.3552	2.5904	2.6394	2.9791	3.0848	3.1186
CFS_2F	1	**0.42424**	**1.3255**	**1.4076**	**1.7131**	**2.0164**	**2.1309**	**2.3080**	**2.4349**	**2.8105**	**2.8391**
	(FEM)	0.42430	1.3258	1.4077	1.7135	2.0164	2.1312	2.3092	2.4360	2.8110	2.8398
	2	**0.34016**	**1.1785**	**1.9369**	**2.1332**	**2.7862**	**2.8188**	**2.8240**	**3.1190**	**3.1298**	**3.6910**
	(FEM)	0.34019	1.1786	1.9370	2.1335	2.7864	2.8189	2.8242	3.1194	3.1306	3.6919
$CCCS_1$	1	**1.2132**	**1.9969**	**2.2352**	**2.2778**	**2.5560**	**3.0175**	**3.0446**	**3.3707**	**3.3757**	**3.4761**
	(FEM)	1.2133	1.9971	2.2354	2.2780	2.5564	3.0180	3.0458	3.3718	3.3768	3.4772
	2	**1.7034**	**2.2952**	**2.8499**	**3.2027**	**3.9873**	**4.0988**	**4.1889**	**4.4929**	**4.6674**	**4.8289**
	(FEM)	1.7034	2.2953	2.8500	3.2029	3.9877	4.0996	4.1896	4.4932	4.6680	4.8296
CCS_2S_2	1	**1.4524**	**1.8541**	**2.1004**	**2.3961**	**2.7218**	**2.8428**	**2.8930**	**3.2008**	**3.4805**	**3.6628**
	(FEM)	1.4525	1.8542	2.1006	2.3964	2.7224	2.8432	2.8936	3.2018	3.4816	3.6646
	2	**2.1514**	**2.8388**	**2.9490**	**3.3642**	**3.7110**	**4.1161**	**4.2226**	**4.7310**	**5.0355**	**5.1148**
	(FEM)	2.1514	2.8390	2.9492	3.3645	3.7112	4.1164	4.2232	4.7316	5.0364	5.1160
S_2FFF	1	**0**	**0.60483**	**0.96018**	**1.2847**	**1.3690**	**1.4235**	**1.7673**	**1.7737**	**2.3317**	**2.4265**
	(FEM)	0	0.60486	0.96020	1.2848	1.3691	1.4236	1.7676	1.7741	2.3324	2.4276
	2	**0**	**0.41073**	**0.97467**	**1.3733**	**2.1777**	**2.5752**	**2.5910**	**2.6476**	**2.8236**	**3.0954**
	(FEM)	0	0.41072	0.97468	1.3734	2.1779	2.5754	2.5912	2.6480	2.8238	3.0958
CS_2CF	1	**1.1517**	**1.8466**	**1.9972**	**2.1771**	**2.2417**	**2.5621**	**2.8357**	**2.9593**	**3.2951**	**3.3763**
	(FEM)	1.1519	1.8471	1.9974	2.1776	2.2420	2.5626	2.8378	2.9600	3.2966	3.3776
	2	**1.6135**	**1.9198**	**2.1271**	**2.8519**	**2.8978**	**3.7994**	**3.8478**	**4.0503**	**4.0772**	**4.4194**
	(FEM)	1.6136	1.9199	2.1273	2.8521	2.8984	3.8006	3.8482	4.0504	4.0776	4.4200
CS_2FF	1	**0.76135**	**0.98940**	**1.0977**	**1.5219**	**1.9179**	**2.0841**	**2.2674**	**2.5091**	**2.6725**	**2.8535**
	(FEM)	0.76138	0.98944	1.0978	1.5222	1.9183	2.0844	2.2682	2.5098	2.6734	2.8546
	2	**0.97671**	**1.3419**	**1.5115**	**2.1949**	**2.4509**	**2.9808**	**3.1459**	**3.3589**	**3.6865**	**4.0105**
	(FEM)	0.97672	1.3420	1.5115	2.1951	2.4511	2.9809	3.1466	3.3592	3.6873	4.0112

Table 4
The first ten dimensionless inplane frequency parameters $\lambda = \omega a\sqrt{\rho(1-\nu^2)/E}$ of a square isotropic plate ($\nu = 0.3$) whose four edges are subjected identical non-uniform elastic supports. In particular, $E_{L\hat{T}}$ stands for an elastically supported edge with triangularly distributed stiffness ($\mu_0(1 - |\xi/L|)$) in both normal and tangent directions; whereas $E_{\hat{L}\hat{T}}$ represents elastic supports with parabolically distributed stiffness $\mu_0[1 - (\xi/L)^2]$ in both directions. For all elastic supports, $\mu_0 = K_0^* E/[a(1-\nu^2)]$ where K_0^* is the dimensionless elastic stiffness taking either 1 or 10^4 in this table.

K_0^*	methods	1	2	3	4	5	6	7	8	9	10
$E_{L\hat{T}}E_{L\hat{T}}E_{\hat{L}\hat{T}}E_{L\hat{T}}$											
1	**SDSM**	**0.85374**	**0.85374**	**1.1786**	**1.4295**	**1.7149**	**1.7405**	**1.7405**	**1.9601**	**1.9741**	**2.1438**
Ritz(trig.) [43]		0.8537	0.8537	1.1786	1.4295	1.7149	1.7405	–	–	–	–
10^4	**SDSM**	**1.7773**	**1.7773**	**2.1174**	**2.5922**	**2.9290**	**2.9470**	**2.9470**	**3.3529**	**3.5558**	**3.5558**
Ritz(trig.) [43]		1.7773	1.7773	2.1174	2.5923	2.929	2.9471	–	–	–	–
$E_{L\hat{T}}E_{\hat{L}\hat{T}}E_{\hat{L}\hat{T}}E_{\hat{L}\hat{T}}$											
1	**SDSM**	**0.85374**	**0.85374**	**1.1786**	**1.4295**	**1.7149**	**1.7405**	**1.7405**	**1.9601**	**1.9741**	**2.1438**
Ritz(trig.) [43]		0.8537	0.8537	1.1786	1.4295	1.7149	1.7405	–	–	–	–
10^4	**SDSM**	**1.7773**	**1.7773**	**2.1174**	**2.5922**	**2.9290**	**2.9470**	**2.9470**	**3.3529**	**3.5558**	**3.5558**
Ritz(trig.) [43]		1.7773	1.7773	2.1174	2.5923	2.929	2.9471	–	–	–	–

where $\xi \in [-L, L]$ is the local coordinate along the corresponding line node. In addition, $\dot{()}$ stands for fixed deformation, i.e., $\dot{()} \equiv 0$. The SDSM are computed with five significant figures, which all match with those obtained by the Trigonometric Ritz method by Dozio [43] wherever available.

Next, we will demonstrate the application of the SDSM to laminated plates subject to both classical BCs and non-uniform elastic supports. Table 5 includes the first ten inplane natural frequencies of a square symmetric cross-ply plate for three cases whose details are given in Fig. 2. The three cases include a fully clamped case and two cases with non-uniform elastic supports as shown in Fig. 2. All SDSM results are accurate to the last digit quoted. It can be seen that all of the first four eigenvalues for the CCCC case coincide with those obtained by Ritz (trig.) method [43] wherever available.

7.2. Applications to engineering composite plate assemblies

So far, the SDSM has been applied to individual plates only. A review of the literature reveals that all existing analytical work has been limited to the free inplane vibration of individual plates, there has been no existing work devoted to that of plate assemblies, let alone the modelling of arbitrary non-uniform elastic supports, mass attachments or coupling constraints. However, all these kinds of problems can be modelled easily and efficiently by the proposed method.

7.2.1. A stepped cantilever laminated plate

The first problem is a stepped cantilever laminated plate as shown in Fig. 3 whose out-of-plane free vibration analysis has already been reported in [56], and now we are focusing on its

Table 5
Dimensionless natural frequencies $\lambda = \omega a\sqrt{\rho(1-\nu_{12}\nu_{21})/E_1}$ of a square symmetric cross-ply plate under three different boundary conditions as illustrated in Fig. 2.

Cases	K_0^*	1	2	3	4	5	6	7	8	9	10
CCCC	–	**1.0646**	**1.1582**	**1.2654**	**1.3107**	**1.3532**	**1.4769**	**1.4956**	**1.6435**	**1.7024**	**1.8336**
	(Ref. [39])	1.0646	1.1582	1.2654	1.3107	–	–	–	–	–	–
$E_{\hat{L}\check{T}}S_2E_{\check{L}\hat{T}}S_2$	0	**0**	**0.27164**	**0.54329**	**0.81493**	**1.0547**	**1.0866**	**1.1607**	**1.2369**	**1.2751**	**1.3103**
	1	**0.70859**	**0.72554**	**0.90925**	**1.0619**	**1.0915**	**1.1620**	**1.3061**	**1.3103**	**1.4947**	**1.5368**
	10	**1.0637**	**1.1044**	**1.1086**	**1.1761**	**1.2409**	**1.3103**	**1.3813**	**1.4951**	**1.5565**	**1.7022**
$E_{\hat{L}\check{T}}$CCC	0	**1.0379**	**1.1029**	**1.2301**	**1.2652**	**1.3530**	**1.4001**	**1.4764**	**1.5963**	**1.6433**	**1.8127**
	1	**1.0610**	**1.1447**	**1.2653**	**1.2848**	**1.3531**	**1.4574**	**1.4767**	**1.6432**	**1.6525**	**1.8335**
	10	**1.0641**	**1.1561**	**1.2654**	**1.3066**	**1.3532**	**1.4769**	**1.4894**	**1.6434**	**1.6937**	**1.8336**

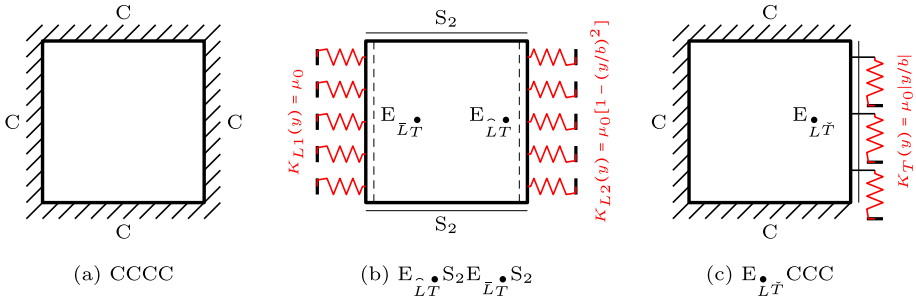

Fig. 2. A square symmetric cross-ply plate ($x \times y = [-a, a] \times [-b, b]$) subject to three different boundary conditions. The plate is composed of five graphite-epoxy laminae [0°/90°/0°/90°/0°] with the material properties: $E_1/E_2 = 20, G_{12} = 0.6E_2$ and $\nu_{12} = 0.25$. The stiffness constants of the elastic supports is $\mu_0 = K_0^* E_1 h/[a(1-\nu_{12}\nu_{21})]$, where K_0^* is a dimensionless stiffness constant taking 0, 1 and 10 as in Table 5.

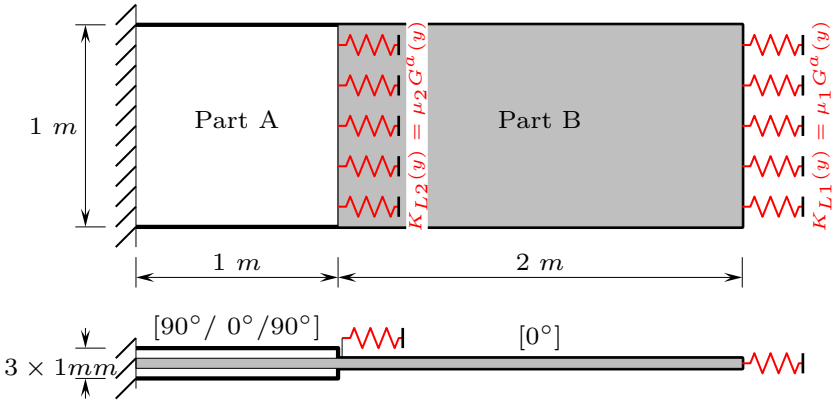

Fig. 3. A stepped cantilever laminated plate subjected to uniform or non-uniform normal elastic supports ($y \in [-b, b]$).

inplane vibration. The structure consists of three laminae with stacking sequence [90°/0°/90°]. Each ply is 1 mm thick and made of T-graphite/epoxy lamina. The top and bottom laminae extend at 1 m from the cantilever edge whereas the middle laminae is extended by a further 2 m. The plate is cantilevered on the left hand edge, and subjected to seven different combinations of classical or non-classical BCs denoted by Cases 1 ~ 7 in Table 6. The uniform or non-uniform elastic supports in the normal direction are applied either along the right end or on the thickness step between Part A and Part B as shown in Fig. 3. Two SDS elements corresponding to Part A and Part B are used in the modelling. The first eight natural frequencies are given in Table 6 for all seven cases. It should be kept in mind that both the structure and the BCs for all seven cases are symmetric with respect to the middle line perpendicular to the clamped edge. A close inspection on the results given in Table 6 will lead to the following conclusions:

(i) Any additional elastic support will increase all the natural frequencies of the structure as expected.

(ii) In such a symmetric configuration, the increase in the natural frequency of the structure caused by the elastic supports is in a descending order with respect to the stiffness distributions: $\mu_0, \mu_0[1-(y/b)^2]$ and $\mu_0(1-|y/b|)$. This is to be expected since the average amplitudes of the above three distributions are in a descending order.

(iii) The same normal elastic support applied along the right end of the plate results in a larger increase in all of the natural frequencies than that applied along the middle line at the thickness step.

7.2.2. Coupled shear walls placed on an elastic foundation and subjected to non-uniform mass attachments

Coupled shear walls are frequently encountered in high rise buildings as an efficient design to resist the lateral forces coming from wind or earthquake [63]. Of course, the FEM can be applied for shear wall analysis but has never been popular due to its relatively low efficiency and high computing cost. Therefore, many attempts [16–18,64,20] have been made by using more efficient

Table 6
The first eight natural frequencies (Hz) of a stepped cantilever composite plate as shown in Fig. 3 for seven cases with different combinations of μ_1, μ_2 and $G^a(y)$. In this table, $\mu_0 = E_1 t/[2b(1-\nu_{12}\nu_{21})]$ where $2b = 1$ m, $t = 0.001$ m, and the plate is made of T-graphite/epoxy lamina with the material properties: $E_1 = 185$ GPa, $E_2 = 10.5$ GPa, $G_{12} = 7.3$ GPa, $\nu_{12} = 0.28$ and $\rho = 1600$ kg/m^3.

Cases	μ_1	μ_2	$G^a(y)$	1	2	3	4	5	6	7	8
1	0	0	–	143.50	444.90	730.09	876.31	1120.4	1278.2	1360.2	1407.8
2	μ_0	0	1	163.71	464.23	758.75	1175.2	1273.9	1297.2	1394.0	1461.3
3	μ_0	0	$1-(y/b)^2$	156.08	455.56	744.55	1153.2	1196.1	1282.1	1382.5	1459.0
4	μ_0	0	$1-\lvert y/b\rvert$	152.90	452.59	740.37	1141.1	1145.4	1281.5	1379.2	1455.3
5	0	μ_0	1	160.32	445.32	730.96	1049.4	1151.9	1280.5	1362.0	1479.5
6	0	μ_0	$1-(y/b)^2$	150.98	445.20	730.64	1002.3	1136.0	1280.2	1361.6	1453.0
7	0	μ_0	$1-\lvert y/b\rvert$	148.45	445.12	730.49	976.08	1131.1	1279.9	1361.3	1438.3

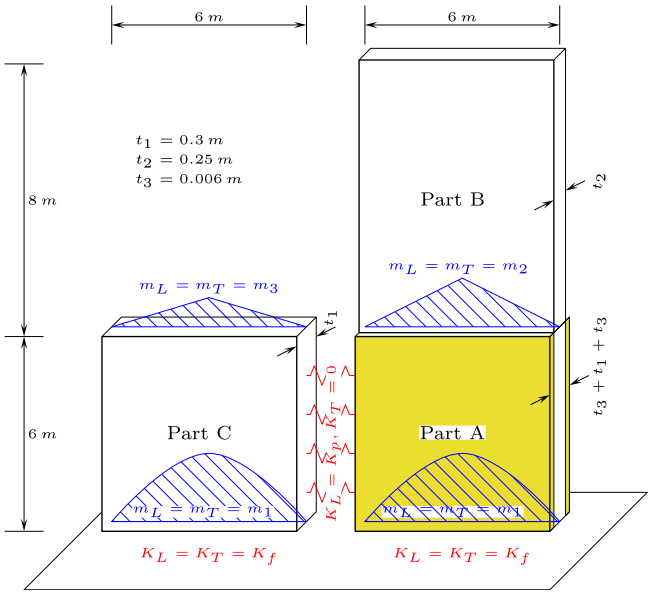

Fig. 4. Coupled shear walls placed on an elastic foundation. The front and back yellow layers are either steel or CFRP sheets to reinforce Part A of the right shear wall. The red springs indicate the elastic coupling constraints between the two shear walls; the blue shaded areas denote the non-uniformly distributed line masses which model the loading coming from floors. The characteristics of the components are given in Table 7.

methods, e.g., finite strip method [16], Rayleigh–Ritz method [17], transfer matrix method [18], continuous-discrete approach [64] and reduced finite element method [20]. Although many existing work [16–18,64] focused on the effects caused by elastic foundations on the shear walls, to the best of our knowledge, there has been no research dealing with non-uniform line masses to model the loading coming from floors. Nevertheless, these floor loadings should never have been neglected since they generally change the dynamic behaviour of the shear walls significantly. On the other hand, in many engineering cases such as earthquake damaged buildings, shear walls need to be reinforced for example, by steel sheets or carbon fibre-reinforced plastic (CFRP) sheets, which have been proved to be mechanically effective. However, there is very few work available in the literature, a recent work was conducted by using the FEM [20]. It is exciting to see that the proposed theory provides a convenient and efficient tool for the modal analysis of coupled shear walls with the capability of considering all above factors.

The coupled shear wall to be investigated using the SDSM in this paper is shown in Fig. 4. In this problem, the coupling between the two shear walls is modelled as a uniform elastic coupling constraint (red spring in Fig. 4) with normal stiffness $K_L = K_p$ and shear stiffness $K_T = 0$ where K_p is given in Table 7. The coupled shear walls are placed on an elastic foundation which has the same stiffness in both vertical and horizontal directions: $K_L = K_T = K_f$ and K_f is also given in Table 7. The left shear wall (Part C) is further subjected to a parabolically distributed mass (m_1) on the floor and a triangularly distributed mass (m_3) on the roof. The floor of the right shear wall (part A) is also subjected to mass m_1 whilst the second floor loading is modelled by a triangular mass m_2. Here, the non-uniform masses m_1, m_2 and m_3 are given in Table 7, with the assumption that all masses exert the same effects in the vertical and horizontal directions, i.e., $m_L = m_T = m_i,\ i = 1, 2, 3$. The material of the shear wall (Parts B, C and the main body of Part A) has the properties: $E_c = 2$ GPa, $\nu = 0.25$, $\rho = 2400$ kg/m^3. Part A is further reinforced on the front and back surfaces by either steel sheets ($E = 200$ GPa, $\nu = 0.3$, $\rho = 7600$ GPa) or CFRP sheets ($E_1 = 138$ GPa, $E_2 = 8.96$ GPa, $G_{12} = 7.1$ GPa, $\nu_{12} = 0.3$, $\rho = 1560$ kg/m^3). It should be noted that the CFRP sheets are placed in such a way that the direction corresponding to E_1 is parallel to the vertical direction to maximise the reinforcement.

Eight cases are considered by using the current SDSM. Different cases have different combinations of foundation stiffness (K_f), elastic coupling stiffness (K_p), mass distribution (m_1, m_2 and m_3) and whether the shear wall (Part A) is reinforced or not, which are indicated in Table 7. The first ten natural frequencies for the eight cases are included in Table 8 and the first four mode shapes of Cases 1, 6

Table 7
Eight different cases investigated for the coupled shear walls as shown in Fig. 4. In this table, $E_c = 2$ GPa and $t_1 = 0.3$ m. ξ represents either x or y, and $2L = 6$ m. In Cases 7 and 8, Part A is reinforced by either steel or CFRP sheets (thickness $t_3 = 0.006$ m) which are applied on the front and back surfaces.

	K_f	K_p	m_1 (kg/m)	m_2 (kg/m)	m_3 (kg/m)	Reinforcement
Case 1	$E_c t_1/2$	$E_c t_1/5$	–	–	–	none
Case 2	$2E_c t_1$	$E_c t_1/5$	–	–	–	none
Case 3	∞	$E_c t_1/5$	–	–	–	none
Case 4	$E_c t_1/2$	$E_c t_1$	–	–	–	none
Case 5	$E_c t_1/2$	$E_c t_1/5$	$5\times10^4[1-(\xi/L)^2]$	–	–	none
Case 6	$E_c t_1/2$	$E_c t_1/5$	$5\times10^4[1-(\xi/L)^2]$	$2\times10^4(1-\lvert\xi/L\rvert)$	$1\times10^4(1-\lvert\xi/L\rvert)$	none
Case 7	$E_c t_1/2$	$E_c t_1/5$	$5\times10^4[1-(\xi/L)^2]$	$2\times10^4(1-\lvert\xi/L\rvert)$	$1\times10^4(1-\lvert\xi/L\rvert)$	Steel (t_3)
Case 8	$E_c t_1/2$	$E_c t_1/5$	$5\times10^4[1-(\xi/L)^2]$	$2\times10^4(1-\lvert\xi/L\rvert)$	$1\times10^4(1-\lvert\xi/L\rvert)$	CFRP (t_3)

Table 8
The first six natural frequencies (Hz) of the coupled shear walls for the eight cases described in Table 7.

	1	2	3	4	5	6	7	8	9	10
Case 1	4.194	14.46	15.14	24.40	28.98	35.69	40.67	42.23	47.78	60.52
Case 2	4.679	15.97	16.67	25.44	35.20	37.65	43.67	46.12	49.49	62.29
Case 3	4.885	16.75	17.27	26.06	37.67	38.94	44.96	47.81	50.07	63.23
Case 4	4.276	14.60	15.14	27.59	29.05	37.37	42.21	43.19	48.38	60.86
Case 5	4.169	12.08	12.60	13.44	14.34	15.26	18.00	18.55	18.63	19.73
Case 6	3.531	9.556	9.965	13.27	14.14	14.67	15.80	16.80	18.53	18.96
Case 7	4.443	11.39	11.94	13.27	14.34	15.87	16.97	18.56	19.87	21.99
Case 8	4.214	11.14	11.23	13.27	14.26	15.09	16.18	18.54	19.76	20.05

and 8 are shown in Fig. 5. The computed results can lead to the following conclusions:

(i) The comparison among Cases 1, 2 and 3 reveals that larger foundation stiffness will lead to higher natural frequencies as expected.
(ii) The elastic coupling stiffness between the two shear walls also exert a positive effect on improving the natural frequencies. This is evident by comparing Cases 1 and 4.
(iii) The floor loadings play a very important role on the natural frequencies of the shear walls which therefore, should not have been neglected in the previous investigations [16–18,64,20]. It is clear from Table 8 that, compared to the unloaded case (Case 1), any mass attached onto the shear walls (Cases 5 and 6) will decrease the natural frequencies; and the reduction in higher frequencies (about 70% decrease) are more remarkable than that in lower frequencies (up to 17% decrease). Moreover, the masses placed onto the higher floor (m_2 and m_3 in Case 6) plays

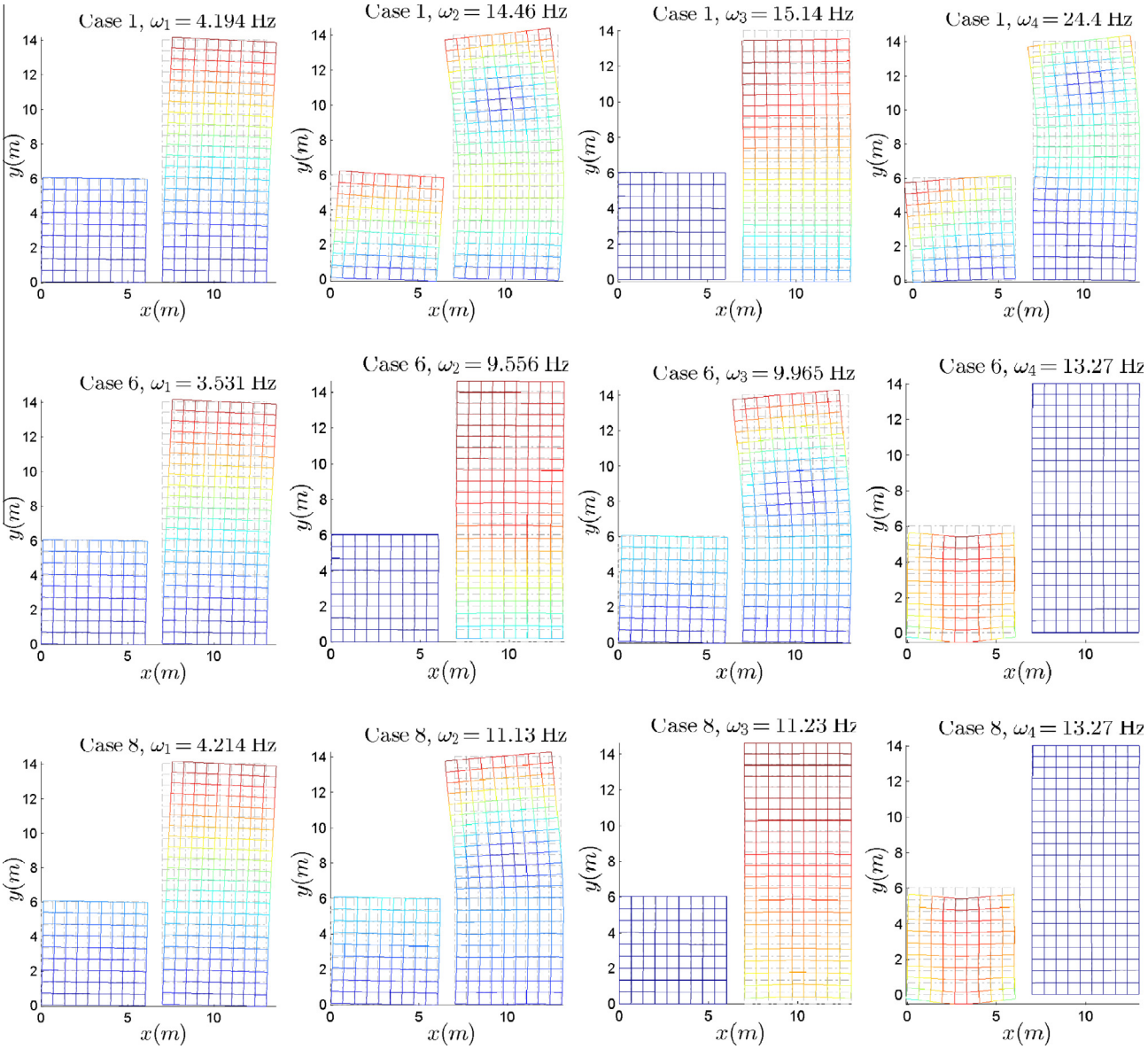

Fig. 5. The first four mode shapes of coupled shear walls as shown in Fig. 4 for the Cases 1,6 and 8 as described in Table 7.

Table 9
The first ten dimensionless elastic natural frequency parameters for the plane strain free vibration of a prismatic orthotropic solid with square cross section subjected to three types of classical BCs.

BCs	$\lambda = 2\omega a/\pi\sqrt{\rho/G_{xy}}$									
CCCC	1	2	3	4	5	6	7	8	9	10
	1.6305	**2.3210**	**2.7225**	**2.7575**	**3.1942**	**3.2238**	**3.2433**	**3.8104**	**3.9590**	**3.9729**
FFFF	4	5	6	7	8	9	10	11	12	13
	1.1106	**1.2443**	**1.2897**	**1.6678**	**1.8024**	**2.0231**	**2.2794**	**2.4289**	**2.6193**	**2.6740**
S_2FS_2F	2	3	4	5	6	7	8	9	10	11
	0.67848	**1.2897**	**1.6522**	**1.7265**	**2.1157**	**2.4298**	**2.6222**	**2.6305**	**2.6845**	**2.8175**

a more significant role (17% decrease) on the fundamental natural frequency than those placed on the lower floor (m_1 in Case 5) with a very small reduction.
(iv) The reinforcements by the steel sheets (Case 7) and the CFRP sheets (Case 8) result in a considerable increase (20–26%) in the first natural frequencies compared to the unreinforced case (Case 6), but less so for higher natural frequencies. In particular, the steel sheets lead to a slightly larger increase in natural frequencies than the CFRP sheets.

7.3. Applications to plane strain free vibration of prismatic orthotropic solids

As mentioned in the Introduction, the SDS formulation developed in this paper is applicable not only to the free inplane vibration of plate assemblies under plane stress assumption, but also applicable to the cross-sectional free vibration of infinite prismatic orthotropic solids under plane strain assumption. However, it should be noted that the reduced stiffnesses in the plane strain vibration problems will be different from that of plane stress ones, see Appendix A. The constitutive relations of plane strain vibration of orthotropic solids are determined by seven independent stiffness constants, which is different from the plane stress vibration determined by four elastic constants only.

Table 9 shows the first ten elastic natural frequencies for the cross-sectional vibration of a prismatic orthotropic solid with square cross section under three different classical BCs, e.g., fully clamped (CCCC), completely free (FFFF) and another case (S_2FS_2F). The material properties of the solid are: $E_2/E_1 = 4$, $E_3/E_1 = 40$, $G_{12}/E_1 = 0.6$, $\nu_{21} = 0.38$, $\nu_{31} = 0.4$, $\nu_{32} = 0.3$. The orthotropic material is placed in such a way that the 3 direction in the material coordinate system is normal to the cross section of the prismatic solid, whereas the 1 and 2 directions are coincide with the x and y directions within the cross section. Again, the first three natural frequencies of the completely free case ('FFFF') and the first natufral frequency of the 'S_2FS_2F' case are zero corresponding to rigid body modes, which are captured by the SDSM but not shown in Table 9.

As the final example, we now apply the current SDSM to investigate the plane strain vibration of an infinite prismatic orthotropic solid as shown in Fig. 6. The solid is made of carbon fibre/epoxy material: $E_1 = 161.0$ GPa, $E_2 = E_3 = 11.38$ GPa, $G_{12} = 5.170$ GPa, $\nu_{12} = \nu_{13} = 0.38$, $\nu_{23} = 0.30$, $\rho = 1560$ kg/m^3. The 1 direction in the material reference system is placed horizontally. The cross section of the solid is 4 cm wide and 1 cm high and is clamped on the leftmost surface. Five cases with/without uniform mass and with/without the presence of crack are considered: In Cases 2–5, there is a uniformly distributed mass placed between 2 and 3 cm away from the clamped surface, see Fig. 6; In Cases 3–5, there is a crack located at 1 cm away from the clamped surface. The mass is denoted by $m(\xi)$; and the cracks are modelled by elastic coupling constraints with parabolically distributed stiffnesses: $K_T(\xi)$ and/or $K_L(\xi)$. Therefore, the five cases are described as following

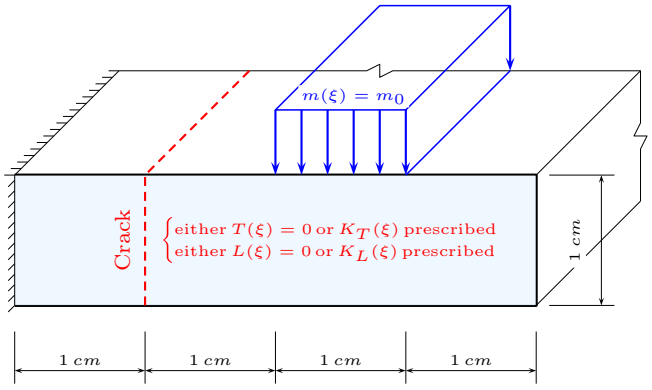

Fig. 6. A cracked infinite prismatic solid made of carbon fibre/epoxy material and subjected to a partially distributed mass attachment. In this figure, $\xi \in [-L, L]$ with $2L = 1$ cm.

$$\text{Case1}: \quad T(\xi) = 0, \quad L(\xi) = 0, \quad m(\xi) = 0, \tag{64a}$$

$$\text{Case2}: \quad T(\xi) = 0, \quad L(\xi) = 0, \quad m(\xi) = m_0, \tag{64b}$$

$$\text{Case3}: \quad K_T(\xi) = K_{T0}[1 - (\xi/L)^2], \quad L(\xi) = 0, \quad m(\xi) = m_0, \tag{64c}$$

$$\text{Case4}: \quad T(\xi) = 0, \quad K_L(\xi) = K_{L0}[1 - (\xi/L)^2], \quad m(\xi) = m_0, \tag{64d}$$

$$\text{Case5}: \quad K_T(\xi) = K_{T0}[1 - (\xi/L)^2], \quad K_L(\xi) = K_{L0}[1 - (\xi/L)^2], \quad m(\xi) = m_0, \tag{64e}$$

where $K_{T0} = K_{L0} = 1 \times 10^{13}$ Pa and $m_0 = 40$ kg/m^2. In particular, Case 1 is a uncracked solid without mass attachment; Case 2 is a uncracked solid with mass attachment; in Case 3, the normal displacements along the crack are assumed to be continuous but the tangent displacement are elastically coupled; in Case 4, the normal displacements along the crack are elastically coupled but the tangent ones are assumed to be continuous; and in Case 5, both normal and tangent displacements on both sides of the crack are elastically coupled. In the SDSM implementation, four square SDSM elements are used to model inplane vibration of the cracked prismatic solids. The first ten inplane natural frequencies for the five cases are given in Table 10 with four significant figures. It is clear that the mass attachment decreases all natural frequencies especially for higher ones. The presence of the crack also lead to a decrease for all natural frequencies. More specifically, the coupling constraint in the normal direction (Case 4) reduces the natural frequencies more significantly than that in the tangent direction (Case 3) with the same stiffness distribution. The first six mode shapes of the cross section for Case 5 are shown in Fig. 7. The crack is clearly seen from the 3rd, 4th and the 5th modes. In addition, the uniform mass attachment causes local vibrations for higher modes, e.g., the 4th, 5th and the 6th modes.

Table 10
The first ten natural frequencies for the plane strain vibration of a prismatic orthotropic solid made of carbon fibre/epoxy material as depicted in Fig. 6. Five cases as described in Eq. (64) are considered.

Cases	Modes (kHz)									
	1	2	3	4	5	6	7	8	9	10
1	7.431	25.31	49.68	63.76	71.84	94.50	109.6	121.8	139.4	141.1
2	5.527	20.74	37.91	38.53	45.22	55.92	66.41	73.13	77.64	79.24
3	5.487	20.60	37.89	38.50	45.21	55.88	66.31	72.48	77.41	79.00
4	3.926	18.35	29.69	37.63	43.74	55.81	65.43	67.68	73.01	78.39
5	3.913	18.17	29.68	37.61	43.74	55.77	65.41	67.54	72.41	78.04

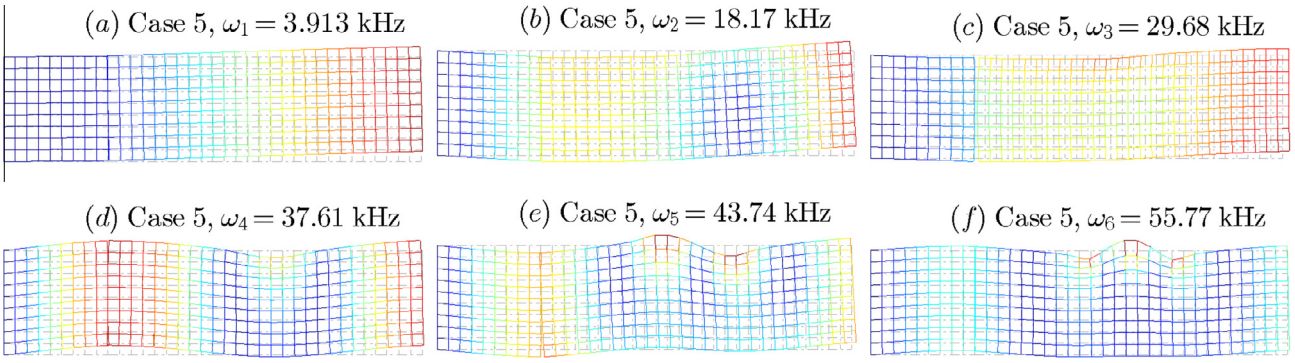

Fig. 7. The first six mode shapes of a cracked prismatic orthotropic solid (depicted in Fig. 6) for Case 5 as given by Eq. (64e).

8. Conclusions

This paper has presented a novel analytical spectral dynamic stiffness method (SDSM) for exact inplane modal analysis of symmetric cross-ply plate assemblies and prismatic orthotropic solids subject to arbitrary boundary conditions, arbitrary non-uniform elastic supports, mass attachments and coupling constraints. The exact shape function of the inplane governing differential equation is first derived by using two types of 1D modified Fourier series. Eventually, the spectral dynamic stiffness (SDS) matrix for the inplane vibration of an element is formulated in a mixed-variable form, which can then be assembled directly to form the global SDS matrix for either the inplane vibration of composite plate assemblies or the cross-sectional vibration of prismatic orthotropic solids. In both cases, the structures can be subjected to any arbitrary classical boundary conditions. Furthermore, the additional inplane SDS matrices generated by any arbitrary non-uniform elastic supports, mass attachments and coupling constraints are formulated in a strong form. Those additional inplane SDS matrices are then superposed directly to the global inplane SDS matrix of the parent structures. Finally, as the solution technique, the Wittrick-William algorithm is enhanced by resolving the mode count problem of a fully clamped element in an elegant and efficient manner. It has been demonstrated that the SDSM method gives exact solutions with prominent computational efficiency. This is attributed to the factor that the inplane vibration of the structures is described accurately in the proposed SDSM by using an extremely few DOFs. Then, the versatility of the method has been further demonstrated by applying the method to a wide range of engineering problems. All results obtained by the SDSM are accurate up to the last digit presented, therefore will serve as benchmark solutions. The current SDSM offers an efficient and accurate technique for the parametric and optimisation analysis on the inplane vibration of a wide range of composite structures.

Acknowledgements

The author appreciates the support given by EPSRC (UK) through a Grant EP/J007706/1 which made this research possible. The author would like to thank Prof. J.R. Banerjee (City University London) for his support thought this work. The author is also grateful to the anonymous referees for their valuable comments on improving the presentation of the manuscript.

Appendix A. The constitutive relations for orthotropic materials in plane stress and plane strain deformation

The constitutive law for an orthotropic material in the lamina reference system can be cast in the following compliance matrix form.

$$\begin{bmatrix} \varepsilon_{11} \\ \varepsilon_{22} \\ \varepsilon_{33} \\ 2\varepsilon_{12} \end{bmatrix} = \begin{bmatrix} 1/E_1 & -\nu_{21}/E_2 & -\nu_{31}/E_3 & 0 \\ -\nu_{12}/E_1 & 1/E_2 & -\nu_{32}/E_3 & 0 \\ -\nu_{13}/E_1 & -\nu_{23}/E_2 & 1/E_3 & 0 \\ 0 & 0 & 0 & 1/G_{12} \end{bmatrix} \begin{bmatrix} \sigma_{11} \\ \sigma_{22} \\ \sigma_{33} \\ \sigma_{12} \end{bmatrix} \tag{A.1}$$

where

$$\frac{\nu_{21}}{\nu_{12}} = \frac{E_2}{E_1}, \quad \frac{\nu_{13}}{\nu_{31}} = \frac{E_1}{E_3}, \quad \frac{\nu_{32}}{\nu_{23}} = \frac{E_3}{E_2}. \tag{A.2}$$

The constitutive equation of an orthotropic material given above will be reduced two special cases under plane deformation, namely, plane stress and plane strain. Both cases can be written in the same matrix form as below

$$\begin{bmatrix} \sigma_{11} \\ \sigma_{22} \\ \sigma_{12} \end{bmatrix} = \begin{bmatrix} Q_{11} & Q_{12} & 0 \\ Q_{21} & Q_{22} & 0 \\ 0 & 0 & Q_{66} \end{bmatrix} \begin{bmatrix} \varepsilon_{11} \\ \varepsilon_{22} \\ 2\varepsilon_{12} \end{bmatrix}, \tag{A.3}$$

but with different expressions for the *reduced stiffnesses* Q_{ij}, which are given as follows.

During plane stress deformation, $\sigma_{33} = 0$. Therefore, the first three rows of Eq.(A.1) are reduced to

$$\begin{bmatrix} \varepsilon_{11} \\ \varepsilon_{22} \end{bmatrix} = \begin{bmatrix} 1/E_1 & -\nu_{21}/E_2 \\ -\nu_{12}/E_1 & 1/E_2 \end{bmatrix} \begin{bmatrix} \sigma_{11} \\ \sigma_{22} \end{bmatrix}. \tag{A.4}$$

Taking the inverse of the coefficient matrix in Eq. (A.4) and that of $1/G_{12}$ in Eq. (A.1), the *plane-stress reduced stiffness* matrix [59] in Eq. (A.3) becomes

$$\begin{bmatrix} Q_{11} & Q_{12} & 0 \\ Q_{21} & Q_{22} & 0 \\ 0 & 0 & Q_{66} \end{bmatrix} = \begin{bmatrix} E_1/(1-\nu_{12}\nu_{21}) & \nu_{21}E_1/(1-\nu_{12}\nu_{21}) & 0 \\ \nu_{12}E_2/(1-\nu_{12}\nu_{21}) & E_2/(1-\nu_{12}\nu_{21}) & 0 \\ 0 & 0 & G_{12} \end{bmatrix}. \tag{A.5}$$

In view of Eq. (A.2), there are four independent engineering constants (e.g., E_1, E_2, ν_{12} and G_{12}) in the reduced stiffness matrix for plane stress deformation.

In plane strain deformation $\varepsilon_{33} = 0$, thus the first three rows of Eq. (A.1) are reduced to

$$\begin{bmatrix} \varepsilon_{11} \\ \varepsilon_{22} \end{bmatrix} = \begin{bmatrix} 1/E_1 - \nu_{13}\nu_{31}/E_1 & -\nu_{21}/E_2 - \nu_{23}\nu_{31}/E_2 \\ -\nu_{12}/E_1 - \nu_{13}\nu_{32}/E_1 & 1/E_2 - \nu_{23}\nu_{32}/E_2 \end{bmatrix} \begin{bmatrix} \sigma_{11} \\ \sigma_{22} \end{bmatrix} \tag{A.6}$$

By taking the inverse of the coefficient matrix in Eq. (A.6) and that of $1/G_{12}$ in Eq. (A.1), the *plane-strain reduced stiffness* matrix in Eq. (A.3) becomes

$$\begin{bmatrix} Q_{11} & Q_{12} & 0 \\ Q_{21} & Q_{22} & 0 \\ 0 & 0 & Q_{66} \end{bmatrix} = \begin{bmatrix} E_1(1-\nu_{23}\nu_{32})/\Delta & E_1(\nu_{21}+\nu_{23}\nu_{31})/\Delta & 0 \\ E_2(\nu_{12}+\nu_{13}\nu_{32})/\Delta & E_2(1-\nu_{13}\nu_{31})/\Delta & 0 \\ 0 & 0 & G_{12} \end{bmatrix} \tag{A.7}$$

where $\Delta = 1 - \nu_{12}\nu_{21} - \nu_{13}\nu_{31} - \nu_{23}\nu_{32} - 2\nu_{12}\nu_{23}\nu_{31}$. According to Eq. (A.2), it can be found that the constitutive relation of an orthotropic material in plane strain depend on seven independent engineering constants (e.g., $E_1, E_2, E_3, \nu_{12}, \nu_{13}, \nu_{23}, G_{12}$), and also the stiffness matrix in Eq. (A.7) is a symmetric matrix.

Appendix B. Two sets of modified Fourier basis functions and the corresponding modified Fourier series

The following two sets of modified Fourier basis functions are adopted in the spectral dynamic stiffness formulation of this paper.

$$\mathcal{T}_l(\gamma_{ls}\xi) = \begin{cases} \cos(\gamma_{ls}\xi) & l = 0 \\ \sin(\gamma_{ls}\xi) & l = 1 \end{cases}, \tag{B.1a}$$

$$\mathcal{T}_l^*(\gamma_{ls}\xi) = \begin{cases} \sin(\gamma_{ls}\xi) & l = 0 \\ \cos(\gamma_{ls}\xi) & l = 1 \end{cases}, \tag{B.1b}$$

where $\gamma_{ls} = (s + l/2)\pi/L$ with $l \in \{0,1\}$ $s \in \mathbb{N}, \mathbb{N} = \{0,1,2,\ldots\}$ and $\xi \in [-L, L]$. Accordingly, two modified Fourier series related to the two sets of basis functions of Eq. (B.1) are given as follows. For any arbitrary 1D function $h(\xi), \xi \in [-L, L]$ subject to *Dirichlet-type* BC (with arbitrary $h(\pm L)$, but $\mathrm{d}_\xi h(\pm L) = 0$), one can write

$$h(\xi) = \sum_{\substack{s\in\mathbb{N} \\ l\in\{0,1\}}} H_{ls} \frac{\mathcal{T}_l(\gamma_{ls}\xi)}{\sqrt{\zeta_{ls}L}}, \quad H_{ls} = \int_{-L}^{L} h(\xi) \frac{\mathcal{T}_l(\gamma_{ls}\xi)}{\sqrt{\zeta_{ls}L}} \mathrm{d}\xi, \tag{B.2}$$

where $\zeta_{ls} = 2$ when $l = s = 0$ and $\zeta_{ls} = 2$ otherwise. For any arbitrary 1D function $h(\xi), \xi \in [-L, L]$ subjected to *Dirichlet-type* BC (with arbitrary $\mathrm{d}_\xi h(\pm L)$, but $h(\pm L) = 0$), one can write

$$h(\xi) = \sum_{\substack{s\in\mathbb{N} \\ l\in\{0,1\}}} H_{ls} \frac{\mathcal{T}_l^*(\gamma_{ls}\xi)}{\sqrt{\zeta_{ls}L}}, \quad H_{ls} = \int_{-L}^{L} h(\xi) \frac{\mathcal{T}_l^*(\gamma_{ls}\xi)}{\sqrt{\zeta_{ls}L}} \mathrm{d}\xi. \tag{B.3}$$

Note that $\sqrt{\zeta_{ls}L}$ appearing in Eqs. (B.2) and (B.3) provides the symmetry of the forward and inverse Fourier transformation and therefore the dependence on the length of integral range $[-L, L]$ is eliminated. The hyperbolic functions $\mathcal{H}_l(\Gamma\xi)$ and its conjugate $\mathcal{H}_l^*(\Gamma\xi)$ encountered when formulating Eq. (37) can be transformed into modified Fourier series by using Eqs. (B.2) and (B.3), respectively. In this way,

$$\mathcal{H}_l(\Gamma\xi) \sum_{s\in\mathbb{N}} \frac{2(-1)^s \Gamma \mathcal{H}_l^*(\Gamma L)}{\sqrt{\zeta_{ls}L}(\Gamma^2 + \gamma_{ls}^2)} \frac{\mathcal{T}_l(\gamma_{ls}\xi)}{\sqrt{\zeta_{ls}L}}, \tag{B.4a}$$

$$\mathcal{H}_l^*(\Gamma\xi) = \sum_{s\in\mathbb{N}} \frac{2(-1)^{s+l+1} \gamma_{ls} \mathcal{H}_l^*(\Gamma L)}{\sqrt{\zeta_{ls}L}(\Gamma^2 + \gamma_{ls}^2)} \frac{\mathcal{T}_l^*(\gamma_{ls}\xi)}{\sqrt{\zeta_{ls}L}}, \tag{B.4b}$$

where $\mathcal{H}_l^*(\Gamma\xi)|_{\xi=L}$ was defined by Eq. (26).

Appendix C. Expressions of the coefficient matrices in the mixed-variable formulation of Eq. (37)

This appendix provides the analytical expressions for the coefficient matrices in Eq. (37). After symbolic manipulation and using the identities of Eq. (23), the four coefficient matrices $\boldsymbol{A}_{TL}^{kj}, \boldsymbol{A}_{TS}^{kj}, \boldsymbol{A}_{NL}^{kj}$ and $\boldsymbol{A}_{NS}^{kj}$ can be expressed in an extremely concise form as follows, which applies for all of the four (k,j) cases with $k,j \in \{0,1\}$.

$$\boldsymbol{A}_{TL}^{kj} = \begin{bmatrix} g_j \mathrm{diag}_n\left[\frac{\beta_{jn}(\Delta_{21}\Upsilon_{21} - \Delta_{22}\Upsilon_{22})}{\Sigma_2}\right] & g_j[\beta_{jn}\Sigma_3\Sigma_7]_{n,m} \\ g_k[\alpha_{km}\Sigma_4\Sigma_8]_{m,n} & g_k \mathrm{diag}_m\left[\frac{\alpha_{km}(\Delta_{11}\Upsilon_{11} - \Delta_{12}\Upsilon_{12})}{\Sigma_1}\right] \end{bmatrix} \tag{C.1a}$$

$$\boldsymbol{A}_{TS}^{kj} = \begin{bmatrix} \mathrm{diag}_n\left[\frac{\Gamma_{21}\Upsilon_{21} - \Gamma_{22}\Upsilon_{22}}{\Sigma_2}\right] & -g_j g_k a_{31}[\alpha_{km}\beta_{jn}\Sigma_7]_{n,m} \\ -g_j g_k a_{31}[\alpha_{km}\beta_{jn}\Sigma_8]_{m,n} & \mathrm{diag}_m\left[\frac{\Gamma_{11}\Upsilon_{11} - \Gamma_{12}\Upsilon_{12}}{\Sigma_1}\right] \end{bmatrix} \tag{C.1b}$$

$$\boldsymbol{A}_{NL}^{kj} = \begin{bmatrix} -\mathrm{diag}_n\left[\frac{\Delta_{21}\delta_{22}\Upsilon_{21} - \Delta_{22}\delta_{21}\Upsilon_{22}}{a_{31}\Sigma_2}\right] & [\Sigma_5\Sigma_7]_{n,m} \\ [\Sigma_5\Sigma_8]_{m,n} & -\mathrm{diag}_m\left[\frac{\Delta_{11}\delta_{12}\Upsilon_{11} - \Delta_{12}\delta_{11}\Upsilon_{12}}{a_{31}\Sigma_1}\right] \end{bmatrix} \tag{C.1c}$$

$$\boldsymbol{A}_{NS}^{kj} = -\begin{bmatrix} g_j \mathrm{diag}_n\left[\frac{\beta_{jn}(\Delta_{21}\Upsilon_{21} - \Delta_{22}\Upsilon_{22})}{\Sigma_2}\right] & g_k[\alpha_{km}\Sigma_4\Sigma_7]_{m,n} \\ g_j[\beta_{jn}\Sigma_3\Sigma_8]_{n,m} & g_k \mathrm{diag}_m\left[\frac{\alpha_{km}(\Delta_{11}\Upsilon_{11} - \Delta_{12}\Upsilon_{12})}{\Sigma_1}\right] \end{bmatrix} \tag{C.1d}$$

where $a_{31} = a_3 + 1$, $g_j = (-1)^j$, $g_k = (-1)^k$ and

$$\Upsilon_{2i} = \mathcal{H}_k(r_{ijn}a)/(\mathcal{H}_k^*(r_{ijn}a)r_{ijn}), \quad \Upsilon_{1i} = \mathcal{H}_j(t_{ikm}b)/(\mathcal{H}_j^*(t_{ikm}b)t_{ikm}),$$

$$\delta_{2i} = a_1 r_{ijn}^2 + a_3\beta_{jn}^2 + \kappa, \quad \delta_{1i} = a_2 t_{ikm}^2 + a_3\alpha_{km}^2 + \kappa,$$

$$\Delta_{2i} = a_1 r_{ijn}^2 + a_3(\beta_{jn}^2 - \kappa), \quad \Delta_{1i} = a_2 t_{ikm}^2 + a_3(\alpha_{km}^2 - \kappa),$$

$$\Gamma_{2i} = a_1 r_{ijn}^2 - \beta_{jn}^2 + \kappa, \quad \Gamma_{1i} = a_2 t_{ikm}^2 - \alpha_{km}^2 + \kappa,$$

$$\Sigma_2 = a_1(r_{1jn}^2 - r_{2jn}^2), \quad \Sigma_1 = a_2(t_{1km}^2 - t_{2km}^2),$$

$$\Sigma_3 = (a_3a_{31} - a_1a_2)\alpha_{km}^2 + a_2(\kappa - \beta_{jn}^2),$$
$$\Sigma_4 = (a_3a_{31} - a_1a_2)\beta_{jn}^2 + a_1(\kappa - \alpha_{km}^2),$$

$$\Sigma_5 = (a_1a_2 - a_3^2)\alpha_{km}^2\beta_{jn}^2 - a_3\kappa(\alpha_{km}^2 + \beta_{jn}^2 - \kappa),$$

$$\Sigma_8 = \Sigma_0 / \left[\sqrt{\zeta_{km}\zeta_{jn}ab}\, a_1(r_{1jn}^2 + \alpha_{km}^2)(r_{2jn}^2 + \alpha_{km}^2)\right],$$

$$\Sigma_7 = \Sigma_0 / \left[\sqrt{\zeta_{km}\zeta_{jn}ab}\, a_2(t_{1km}^2 + \beta_{jn}^2)(t_{2km}^2 + \beta_{jn}^2)\right],$$

where $\Sigma_0 = 2(-1)^{m+n}$, and the hyperbolic functions $\mathcal{H}$ and $\mathcal{H}^*$ were defined in Eq. (26). In Eq. (C.1), '$\mathrm{diag}_n[\cdot]$' represents a diagonal matrix whose diagonal terms are expressed by '$\cdot$' with the subscript n varying from 0 to ∞, whereas '$[\cdot]_{n,m}$' stands for a matrix whose

entries are '·' with n (row number) and m (column number) taking from 0 to ∞. Similarly, it is easy to understand the notations 'diag$_m[\cdot]$' and '$[\cdot]_{m,n}$'. It should be emphasised that since the DOFs corresponding to S_{aj0}, T_{aj0} (when $j=0$) and S_{bk0}, T_{bk0} (when $k=0$) in Eq. (38)) have been removed, the corresponding rows and columns of the $\boldsymbol{A}^{kj}$ matrices also should be removed accordingly. Now if we introduce the notations $\boldsymbol{A}^{kj}(i,:)=[]$ and $\boldsymbol{A}^{kj}(:,l)=[]$ to denote respectively the removal of the ith row and the lth column of the matrix $\boldsymbol{A}^{kj}$, the removal should be applied as follows

$$\boldsymbol{A}^{kj}_{T\cdot}(1,:)=[] \text{ when } j=0, \quad \boldsymbol{A}^{kj}_{T\cdot}(N+1,:)=[] \text{ when } k=0, \tag{C.2a}$$

$$\boldsymbol{A}^{kj}_{S\cdot}(:,1)=[] \text{ when } j=0, \quad \boldsymbol{A}^{kj}_{S\cdot}(:,N+1)=[] \text{ when } k=0, \tag{C.2b}$$

where the subscript '·' in Eq. (C.2a) stands for either L or S; the '·' in Eq. (C.2b) represents either T or N.

Appendix D. The analytical expressions of G^a matrices for some typical functions

This appendix provides the analytical expressions of the $\boldsymbol{G}^a$ matrices for some typical functions based on Eq. (53). (The corresponding expressions based on Eq. (52) have been already given in Appendix A of [58].) The notations used here will follow the same fashion as in [58]. If S terms are adopted in the series solution ($s\in[0,S-1]$), then diag$(\cdot)_{S^1}$ is used to denote a diagonal matrix with the integer 's' in expression '·' taking $s\in[1,S-1]$. Similarly, $[\cdot]_{S^0,S^1}$ stands for a matrix with '·' taking $r\in[0,S-1]$ and $s\in[1,S-1]$; $[\cdot]_{S^1,S^1}$ denotes a matrix with '·' taking $r\in[1,S-1], s\in[1,S-1]$ and so on. Similar to [58], for symmetric distribution functions $G^a(\xi), \boldsymbol{G}^a_{01}=\boldsymbol{O}, \boldsymbol{G}^a_{10}=\boldsymbol{O}$ whereas $\boldsymbol{G}^a_{00}$ and $\boldsymbol{G}^a_{11}$ are derived from Eq. (53), whose analytical expressions are given below for some typical symmetric (even) functions $G^a(\xi)$.

(1) For constant function $G^a(\xi)=1, \boldsymbol{G}^a_{00}=\text{diag}(1)_{S^1}$ and $\boldsymbol{G}^a_{11}=\text{diag}(1)_{S^0}$.

(2) For parabolic function $G^a(\xi)=(\xi/L)^2$, $\boldsymbol{G}^a_{00}=\left[\frac{8(-1)^{r+s}rs}{\left(\pi(r^2-s^2)\right)^2}\right]_{S^1,S^1}$ except for the diagonal terms $\boldsymbol{G}^a_{00}(r,s)=\left[1/3-1/(2\pi^2s^2)\right]$ for $r=s\in[1,S-1]$; and $\boldsymbol{G}^a_{11}=\left[\frac{2(-1)^{r+s}(1+2r)(1+2s)}{(\pi(r-s)(1+r+s))^2}\right]_{S^0,S^0}$ except for the diagonal terms $\boldsymbol{G}^a_{11}(r+1,s+1)=\left[1/3-2/(\pi s_2)^2\right]$ for $r=s\in[0,S-1]$ and where $s_2=1+2s$.

(3) For cosine function $G^a(\xi)=\cos(\pi\xi/(2L))$, $\boldsymbol{G}^a_{00}=\left[-\frac{32(-1)^{r+s}rs}{\pi(16r^4+(1-4s^2)^2-8r^2(1+4s^2))}\right]_{S^1,S^1}$ except for the diagonal terms $\boldsymbol{G}^a_{00}(r,s)=-32s^2/\left[\pi(1-16s^2)\right]$ for $r=s\in[1,S-1]$; and $\boldsymbol{G}^a_{11}=\left[\frac{8(-1)^{r+s}(1+2r)(1+2s)}{\pi\left(4(r-s)^2-1\right)(1+2r+2s)(3+2r+2s)}\right]_{S^0,S^0}$ except for the diagonal terms $\boldsymbol{G}^a_{11}(r+1,s+1)=8(1+2s)/[\pi(1+4s)(3+4s)]$ for $r=s\in[0,S-1]$.

For antisymmetric distribution functions $G^a(\xi), \boldsymbol{G}^a_{00}=\boldsymbol{O}, \boldsymbol{G}^a_{11}=\boldsymbol{O}$ whereas $\boldsymbol{G}^a_{01}$ and $\boldsymbol{G}^a_{10}$ are derived from Eq. (53), whose analytical expressions are given below for some typical antisymmetric (odd) functions $G^a(\xi)$.

(1) For linear function $G^a(\xi)=\xi/L$, $\boldsymbol{G}^a_{01}=\left[-32(-1)^{r+s}4s_2/\left(\pi(-4r^2+s_2^2)\right)^2\right]_{S^1,S^0}$.

(2) For sine function $G^a(\xi)=\sin(\pi\xi/(2L))$, $\boldsymbol{G}^a_{01}=\text{diag}(-1/2)_{S^0}$.

For above two odd functions, the removal procedure as in Eq. (C.2) should also be applied such that: $\boldsymbol{G}^a_{01}(1,:)=[]$, and finally $\boldsymbol{G}^{a\ T}_{10}=\boldsymbol{G}^a_{01}$.

References

[1] Wittrick WH, Williams FW. Buckling and vibration of anisotropic or isotropic plate assemblies under combined loadings. Int J Mech Sci 1974;16(4):209–39. http://dx.doi.org/10.1016/0020-7403(74)90069-1.

[2] Bercin AN, Langley RS. Application of the dynamic stiffness technique to the in-plane vibrations of plate structures. Comp Struct 1996;59(5):869–75.

[3] Boscolo M, Banerjee JR. Dynamic stiffness formulation for composite Mindlin plates for exact modal analysis of structures. Part I: theory. Comp Struct 2012;96–97:61–73. http://dx.doi.org/10.1016/j.compstruc.2012.01.002.

[4] Fazzolari FA, Boscolo M, Banerjee JR. An exact dynamic stiffness element using a higher order shear deformation theory for free vibration analysis of composite plate assemblies. Compos Struct 2013;96:262–78. http://dx.doi.org/10.1016/j.compstruct.2012.08.033.

[5] Boscolo M, Banerjee JR. Layer-wise dynamic stiffness solution for free vibration analysis of laminated composite plates. J Sound Vib 2014;333(1):200–27. http://dx.doi.org/10.1016/j.jsv.2013.08.031.

[6] Guyader JL, Boisson C, Lesueur C. Energy transmission in finite coupled plates, part I: Theory. J Sound Vib 1982;81(1):81–92. http://dx.doi.org/10.1016/0022-460X(82)90178-X.

[7] Boisson C, Guyader JL, Millot P, Lesueur C. Energy transmission in finite coupled plates, part II: application to an L shaped structure. J Sound Vib 1982;81(1):93–105. http://dx.doi.org/10.1016/0022-460X(82)90179-1.

[8] Lyon RH. In-plane contribution to structural noise transmission. Noise Control Eng J 1986;26(1):22–7.

[9] Langley RS, Bercin AN. Wave intensity analysis of high frequency vibrations. Philos Trans R Soc A 1994;346(1681):489–99. http://dx.doi.org/10.1098/rsta.1994.0031.

[10] Bercin AN. An assessment of the effects of in-plane vibrations on the energy flow between coupled plates. J Sound Vib 1996;191(5):661–80. http://dx.doi.org/10.1006/jsvi.1996.0149.

[11] Tomikawa Y, Takano T, Umeda H. Thin rotary and linear ultrasonic motors using a double-mode piezoelectric vibrator of the first longitudinal and second bending modes. Jpn J Appl Phys 1992;31:3073–6.

[12] Manceau J, Bastien F. Linear motor using a quasi-travelling wave in a rectangular plate. Ultrasonics 1996;34(2–5):257–60. http://dx.doi.org/10.1016/0041-624X(95)00080-M.

[13] Lu C, Xie T, Zhou T, Chen Y. Study of a new type linear ultrasonic motor with double-driving feet. Ultrasonics 2006;44(SUPPL.):585–9.

[14] Zhao C. ltrasonic Motors. Berlin, Heidelberg: Springer Berlin Heidelberg; 2011. http://dx.doi.org/10.1007/978-3-642-15305-1.

[15] Coull A, Mukherjee PR. Natural vibrations of shear wall buildings on flexible supports. Earthquake Eng Struct Dyn 1978;6:295–316. http://dx.doi.org/10.1002/eqe.4290060305.

[16] Cheung YK. Free vibration of frame shear wall structures on flexible foundations. Earthquake Eng Struct Dyn 1979;7:355–67.

[17] Balendra T. Free vibration of a shearwall-frame building on an elastic foundation. J Sound Vib 1984;96(4):437–46. http://dx.doi.org/10.1016/0022-460X(84)90631-X.

[18] Syngellakis S, Papoulia KD. A transfer matrix approach to free vibrations of coupled shear walls. Eng Struct 1987;9(4):265–71.

[19] Kuang JS, Chau CK. Dynamic analysis of stiffened coupled shear walls. Eleventh World Conference on Earthquake Engineering. p. 1964.

[20] Meftah SA, Tounsi A. Lateral stiffness and vibration characteristics of damaged RC coupled shear walls strengthened with thin composite plates. Build Environ 2007;42(10):3596–605. http://dx.doi.org/10.1016/j.buildenv.2006.10.049.

[21] Koshiba M, Hasegawa K, Suzuki M. Finite-element solution of horizontally polarized shear wave scattering in an elastic plate. IEEE Trans Ultrason Ferroelectr Freq Control 1987;34(4):461–6. http://dx.doi.org/10.1109/T-UFFC.1987.26967.

[22] Alleyne DN, Cawley P. The interaction of lamb waves with defects. IEEE Trans Ultrason Ferroelectr Freq Control 1992;39(3):381–97. http://dx.doi.org/10.1109/58.143172.

[23] Cawley P, Alleyne DN. The use of Lamb waves for the long range inspection of large structures. Ultrasonics 1996;34(2–5):287–90. http://dx.doi.org/10.1016/0041-624X(96)00024-8.

[24] Ditri JJ. Some results on the scattering of guided elastic SH waves from material and geometric waveguide discontinuities. J Acoust Soc Am 1996;100(5):3078–87. http://dx.doi.org/10.1121/1.417119.

[25] Lowe MJS, Diligent O. Low-frequency reflection characteristics of the s0 lamb wave from a rectangular notch in a plate. J Acoust Soc Am 2002;111(1 Pt 1):64–74. http://dx.doi.org/10.1121/1.1424866.

[26] Cawley P, Adams RD. The location of defects in structures from measurements of natural frequencies. J Strain Anal Eng Des 2007;14(2):49–57. http://dx.doi.org/10.1243/03093247V142049.

[27] Tsiatas G, Gazetas G. Plane-strain and shear-beam free vibration of earth dams. Int J Soil Dyn Earthquake Eng 1982;1(4):150–60. http://dx.doi.org/10.1016/0261-7277(82)90018-3.

[28] Ahmed N. Axisymmetric plane-strain vibrations of a thick-layered orthotropic cylindrical shell. J Acoust Soc Am 1966;40(6):1509–16. http://dx.doi.org/10.1121/1.1910256.
[29] Ding HJ, Wang HM, Hou PF. The transient responses of piezoelectric hollow cylinders for axisymmetric plane strain problems. Int J Solids Struct 2003;40(1):105–23. http://dx.doi.org/10.1016/S0020-7683(02)00525-5.
[30] Dong SB, Nelson RB. On natural vibrations and waves in laminated orthotropic plates. J Appl Mech 1972;39(3):739. http://dx.doi.org/10.1115/1.3422782.
[31] Dong SB, Goetschel DB. Edge effects in laminated composite plates. J Appl Mech 1982;49:129–35.
[32] Dong SB, Huang KH. Edge vibrations in laminated composite plates. J Appl Mech 1985;52:433–8.
[33] Gorman DJ. Accurate in-plane free vibration analysis of rectangular orthotropic plates. J Sound Vib 2009;323(1–2):426–43. http://dx.doi.org/10.1016/j.jsv.2008.12.021.
[34] Boscolo M, Banerjee JR. Dynamic stiffness method for exact inplane free vibration analysis of plates and plate assemblies. J Sound Vib 2011;330(12):2928–36. http://dx.doi.org/10.1016/j.jsv.2010.12.022.
[35] Wang G, Wereley NM. Free in-plane vibration of rectangular plates. AIAA J 2002;40(5):953–9. http://dx.doi.org/10.2514/2.1732.
[36] Xing YF, Liu B. Exact solutions for free in-plane vibrations of rectangular plates. Int J Mech Sci 2009;51:246–55. http://dx.doi.org/10.1016/j.ijmecsci.2008.12.009.
[37] Liu B, Xing YF. Exact solutions for free in-plane vibrations of rectangular plates. Acta Mech Solida Sin 2011;24(6):556–67. http://dx.doi.org/10.1016/S0894-9166(11)60055-4.
[38] Liu B, Xing YF. Comprehensive exact solutions for free in-plane vibrations of orthotropic rectangular plates. Eur J Mech, A/Solids 2011;30(3):383–95. http://dx.doi.org/10.1016/j.euromechsol.2011.01.003.
[39] Dozio L. In-plane free vibrations of single-layer and symmetrically laminated rectangular composite plates. Compos Struct 2011;93(7):1787–800. http://dx.doi.org/10.1016/j.compstruct.2011.01.021.
[40] Ghorbel O, Casimir JB, Hammami L, Tawfiq I, Haddar M. In-plane dynamic stiffness matrix for a free orthotropic plate. J Sound Vib 2016;364:234–46. http://dx.doi.org/10.1016/j.jsv.2015.11.028.
[41] Papkov SO. A new method for analytical solution of inplane free vibration of rectangular orthotropic plates based on the analysis of infinite systems. J Sound Vib 2016:1–18. http://dx.doi.org/10.1016/j.jsv.2016.01.025.
[42] Bardell NS, Langley RS, Dunsdon JM. On the free in-plane vibration of isotropic rectangular plates. J Sound Vib 1996;191(3):459–67. http://dx.doi.org/10.1006/jsvi.1996.0134.
[43] Dozio L. Free in-plane vibration analysis of rectangular plates with arbitrary elastic boundaries. Mech Res Commun 2010;37(7):627–35. http://dx.doi.org/10.1016/j.mechrescom.2010.09.003.
[44] Nefovska-Danilovic M, Petronijevic M. In-plane free vibration and response analysis of isotropic rectangular plates using the dynamic stiffness method. Comp Struct 2015;152:82–95. http://dx.doi.org/10.1016/j.compstruc.2015.02.001.
[45] Mohazzab AH, Dozio L. A spectral collocation solution for in-plane eigenvalue analysis of skew plates. Int J Mech Sci 2015;94–95:199–210. http://dx.doi.org/10.1016/j.ijmecsci.2015.03.008.
[46] Gorman DJ. Free in-plane vibration analysis of rectangular plates with elastic support normal to the boundaries. J Sound Vib 2005;285(4–5):941–66. http://dx.doi.org/10.1016/j.jsv.2004.09.017.
[47] Zhang Y, Du J, Yang T, Liu Z. A series solution for the in-plane vibration analysis of orthotropic rectangular plates with elastically restrained edges. Int J Mech Sci 2014;79:15–24. http://dx.doi.org/10.1016/j.ijmecsci.2013.11.018.
[48] Shi D, Wang Q, Shi X, Pang F. A series solution for the in-plane vibration analysis of orthotropic rectangular plates with non-uniform elastic boundary constraints and internal line supports. Arch Appl Mech 2015;85(1):51–73. http://dx.doi.org/10.1007/s00419-014-0899-x.
[49] Ilanko S. Penalty methods for finding eigenvalues of continuous systems: emerging challenges and opportunities. Comp Struct 2012;104–105:50–4. http://dx.doi.org/10.1016/j.compstruc.2012.02.017.
[50] Xing YF, Liu B. High-accuracy differential quadrature finite element method and its application to free vibrations of thin plate with curvilinear domain. Int J Numer Methods Eng 2009;80:1718–42. http://dx.doi.org/10.1002/nme.2685.
[51] Fantuzzi N, Tornabene F. Strong formulation finite element method for arbitrarily shaped laminated plates Part I. Theor Anal 2014;1(2):125–43. http://dx.doi.org/10.12989/aas.2014.1.2.125.
[52] Fantuzzi N, Tornabene F. Strong formulation isogeometric analysis (SFIGA) for laminated composite arbitrarily shaped plates. Compos Part B: Eng 2016;96:173–203. http://dx.doi.org/10.1016/j.compositesb.2016.04.034.
[53] Liu C, Liu B, Xing YF, Reddy JN, Neves AMA, Ferreira AJM. In-plane vibration analysis of plates in curvilinear domains by a differential quadrature hierarchical finite element method. Meccanica 2016. http://dx.doi.org/10.1007/s11012-016-0426-y.
[54] Liu X, Banerjee JR. Free vibration analysis for plates with arbitrary boundary conditions using a novel spectral-dynamic stiffness method. Comp Struct 2016;164:108–26. http://dx.doi.org/10.1016/j.compstruc.2015.11.005.
[55] Liu X, Banerjee JR. An exact spectral-dynamic stiffness method for free flexural vibration analysis of orthotropic composite plate assemblies – Part I: theory. Compos Struct 2015;132:1274–87. http://dx.doi.org/10.1016/j.compstruct.2015.07.020.
[56] Liu X, Banerjee JR. An exact spectral-dynamic stiffness method for free flexural vibration analysis of orthotropic composite plate assemblies – Part II: applications. Compos Struct 2015;132:1288–302. http://dx.doi.org/10.1016/j.compstruct.2015.07.022.
[57] Liu X, Banerjee JR. A spectral dynamic stiffness method for free vibration analysis of plane elastodynamic problems (under review), Mechanical Systems and Signal Processing.
[58] Liu X, Kassem HI, Banerjee JR. An exact spectral dynamic stiffness theory for composite plate-like structures with arbitrary non-uniform elastic supports, mass attachments and coupling constraints. Compos Struct 2016;142:140–54. http://dx.doi.org/10.1016/j.compstruct.2016.01.074.
[59] Reddy JN. Mechanics of laminated composite plates and shells theory and analysis. 2nd ed. CRC Press; 2003.
[60] Wittrick WH, Williams FW. A general algorithm for computing natural frequencies of elastic structures. Q J Mechan Appl Math 1971;XXIV(3):263–84. http://dx.doi.org/10.1093/qjmam/24.3.263.
[61] Sylvester JJ. A demonstration of the theorem that every homogeneous quadratic polynomial is reducible by real orthogonal substitutions to the form of a sum of positive and negative squares 1852. http://dx.doi.org/10.1080/14786445208647087.
[62] Hardy GH. On the presentation of a number as the sum of any number of squares, and in particular of five. Trans Am Math Soc 1920;17:255–84.
[63] Balendra T. Vibration of buildings to wind and earthquake loads. London: Springer-Verlag; 1993.
[64] Li GQ, Choo BS. A continuous-discrete approach to the free vibration analysis of stiffened pierced walls on flexible foundations. Int J Solids Struct 1996;33(2):249–63. http://dx.doi.org/10.1016/0020-7683(95)00028-9.